Published in final edited form as:
Ultrasound Med Biol. 2010 February ; 36(2): 250. doi:10.1016/j.ultrasmedbio.2009.09.010.

Shock-induced heating and millisecond boiling in gels and tissue due to high intensity focused ultrasound

Michael S. Canney[a], **Vera A. Khokhlova**[a,b], **Olga V. Bessonova**[b], **Michael R. Bailey**[a], and **Lawrence A. Crum**[a]

[a] Center for Industrial and Medical Ultrasound, Applied Physics Laboratory, University of Washington, Seattle, WA 98105

[b] Department of Acoustics, Faculty of Physics, Moscow State University, Moscow, 119991, Russia

Abstract

Nonlinear propagation causes high intensity ultrasound waves to distort and generate higher harmonics, which are more readily absorbed and converted to heat than the fundamental frequency. Although such nonlinear effects have previously been investigated and found not to significantly alter high intensity focused ultrasound (HIFU) treatments, two results reported here change this paradigm. One is that at clinically relevant intensity levels, HIFU waves not only become distorted but form shock waves in tissue. The other is that the generated shock waves heat the tissue to boiling in much less time than predicted for undistorted or weakly distorted waves. In this study, a 2-MHz HIFU source operating at peak intensities up to 25,000 W/cm^2 was used to heat transparent tissue-mimicking phantoms and *ex vivo* bovine liver samples. Initiation of boiling was detected using high-speed photography, a 20-MHz passive cavitation detector, and fluctuation of the drive voltage at the HIFU source. The time to boil obtained experimentally was used to quantify heating rates and was compared to calculations using weak shock theory and the shock amplitudes obtained from nonlinear modeling and from measurements with a fiber optic hydrophone. As observed experimentally and predicted by calculations, shocked focal waveforms produced boiling in as little as 3 ms and the time to initiate boiling was sensitive to small changes in HIFU output. Nonlinear heating due to shock waves is therefore important to HIFU and clinicians should be aware of the potential for very rapid boiling since it alters treatments.

Keywords

HIFU; hifu intensity focused ultrasound; fiber optic hydrophone; KZK; cavitation; boiling; nonlinear acoustics; weak shock theory

Introduction

High intensity focused ultrasound (HIFU) is being used clinically to thermally coagulate benign or malignant tissue (Hill et al. 2004, Clement et al. 2005). One method that has been used in modern HIFU protocols to accelerate treatments is to operate at higher intensity levels so that

Corresponding Author: Michael Canney, Center for Industrial and Medical Ultrasound, Applied Physics Laboratory, University of Washington, 1013 NE 40th St, Seattle, WA 98105, mcanney@u.washington.edu, Telephone: 206-543-1324.

exposure durations, which are typically on the order of seconds, can be reduced (Kennedy 2005, Wu et al. 2004). When higher intensities are used, nonlinear propagation effects increase and result not only in waveform distortion and generation of higher harmonics, but at sufficient levels, in the formation of shock waves (Filonenko and Khokhlova 2001, Dalecki et al. 1991). The presence of shock waves increases the conversion of acoustic energy to heat in tissue. The hypothesis of this work is that shock waves form in tissue at clinically relevant HIFU output levels; furthermore, the loss at the shocks creates sufficient heating to cause boiling well within a clinical exposure duration.

Amplitude-dependent propagation effects are well described by nonlinear acoustic theory (Hamilton and Blackstock 1998). Higher pressure portions of the wave travel faster than lower pressure portions, leading to distortion of the temporal waveform. In the frequency domain, this distortion produces higher harmonics of the fundamental frequency that are more readily absorbed and converted to heat. Nonlinear distortion effects accumulate as the wave propagates and are accelerated by an increase of the wave amplitude. In focused fields, nonlinear effects are the strongest within the focal zone, where the amplitudes are the highest. Sufficient distortion of the wave leads to formation of a shock front, which is a near discontinuity in pressure that generates not just a few but tens or hundreds of harmonics in the frequency domain. Shock formation leads to a significant increase in absorption relative to that of harmonic or even weakly distorted nonlinear waves. The propagation and absorption of shocks can be described using weak shock theory, which has been used for 40 years in underwater and atmospheric acoustics (Pierce 1991, Hamilton and Blackstock 1998).

Although medical ultrasound devices have been observed to produce shock waves in fluids (Duck and Starritt 1984, Cleveland et al. 1998, Canney et al. 2008, Zhou et al. 2006), there has been debate as to whether shock waves *form* in tissue. Shock formation may not be observed in tissue because nonlinear acoustic effects are weakened by loss of amplitude due to degradation of focusing in inhomogeneous tissue and due to tissue absorption. Yet, in previous work with a strongly focused 2-MHz HIFU source, shock waves were measured in both water and in tissue-mimicking phantoms at peak intensities of 6,000 W/cm^2 and higher (Canney et al. 2008). For less focused clinical and laboratory transducers, shock waves were measured and predicted by modeling in water at peak intensities as low as 1500 W/cm^2 (Filonenko and Khokhlova 2001, Pishchalnikov et al. 2002). Since many new clinical HIFU devices operate at peak *in situ* intensities of up to 25,000 W/cm^2 (Kennedy 2005, Wu et al. 2004), shock waves are likely to be present.

Although shock wave formation was not explicitly considered, nonlinear acoustic propagation has previously been studied and shown to have negligible effects on HIFU treatments (Clarke and ter Haar 1999, Hynynen 1987). In HIFU fields with or without shock formation, nonlinear effects concentrate additional heating into a smaller volume. This additional localized heating spreads over time due to thermal diffusion, thereby producing a treated volume similar to that predicted assuming linear acoustic propagation. However, if the extra localized heating is sufficient to raise temperatures to 100°C, the resultant boiling will affect the HIFU treatment. Two major effects that occur are mechanical disruption of the lesion core and increased scattering of ultrasound energy. Such scattering has been observed to produce echogenic regions in ultrasound images and to shift lesion growth towards the HIFU transducer (Khokhlova et al. 2006, Watkin et al. 1996, Meaney et al. 2000). The effects of boiling activity may be either beneficial or detrimental depending on the specific HIFU treatment protocol being used; nevertheless, if shock waves accelerate heating during treatments, these effects may happen much more quickly than either intended or detected.

In our preliminary studies, boiling onset was measured in tissue-mimicking gel phantoms after only 40 ms of HIFU shock-wave-induced heating (Khokhlova et al. 2007). Furthermore, *in*

vivo studies have shown that bubbles were detected after only 30 ms of heating and were speculated to be caused by tissue boiling (Rabkin et al. 2006).

The goal of this paper is to present evidence that shock waves occur in tissue and cause enhanced heating and rapid boiling at clinically relevant exposure levels; furthermore, an approach for quantifying the heating caused by shocks is described. Shock waves were measured and modeled in both a tissue phantom and *ex vivo* tissue. The onset of boiling was visually observed using a high-speed digital camera in transparent tissue phantoms and detected acoustically in both phantoms and *ex vivo* tissue samples. The detected boiling was used as an indication of focal temperatures of 100°C (no superheating was assumed) and the time to boil was used to quantify heating rates. Heating rates and the time to boil were also estimated analytically using weak shock theory and the shocked waveforms either measured with a fiber optic hydrophone or modeled with a Khokhlov-Zabolotskaya-Kuznetsov (KZK)- type equation. Analytic estimates were compared to the experimentally observed time to boil and to the results of direct numerical simulations of the acoustic field, heat deposition, and temperature. An important result of this paper is that the onset of boiling was both measured and predicted to occur after only several milliseconds of HIFU heating in tissue phantom and *ex vivo* tissue. Since boiling may have a significant impact on treatment outcomes, users of HIFU devices are cautioned to consider the potential occurrence of shock waves and corresponding rapid tissue heating in their therapy protocols.

Materials and Methods

Theory

A full numerical "nonlinear model" and two simpler models—a "linear model" and a "weak shock" estimate—are described below and used to calculate acoustic pressures, intensities, and heating rates in tissue phantoms and liver samples. The nonlinear model was refined from our previous work (Khokhlova et al. 2006, Canney et al. 2008). Equations for calculating temperature rise either neglecting or including thermal diffusion are also described. The results from these separate solution methods are compared in the Results Section.

Nonlinear acoustic model

Numerical modeling of the acoustic field of the HIFU source was performed using a KZK-type nonlinear parabolic equation

$$\frac{\partial}{\partial\tau}\left[\frac{\partial p}{\partial z}-\frac{\beta}{\rho_0 c_0^3}p\frac{\partial p}{\partial\tau}-L_{abs}(p)\right]=\frac{c_0}{2}\Delta_\perp p, \tag{1}$$

where p is the acoustic pressure, z is the propagation coordinate along the axis of the beam, $\tau = t - z/c_0$ is the retarded time, c_0 is the sound speed, ρ_0 is the ambient density of the medium, β is the coefficient of nonlinearity, $\Delta_\perp$ is the Laplacian with respect to the transverse coordinate r, L_{abs} is the linear operator that accounts for frequency-dependent absorption and dispersion properties of the propagation medium (Zabolotskaya and Khokhlov 1969, Kuznetsov 1971, Filonenko and Khokhlova 2001). A combined time- and frequency- domain approach was used in this work to model the nonlinearity, absorption, and diffraction terms in Eq. (1). Both the temporal waveform $p(z, r, \tau)$ and its spectral representation were used in modeling and were related by the Fourier transform

$$p(z,r,\tau)=\sum_{-\infty}^{\infty}c_n(z,r)\cdot e^{-in2\pi f_0\tau}, \tag{2}$$

where c_n is the complex amplitude of the nth harmonic. The initial pressure waveform at the source was a harmonic signal of the fundamental frequency f_0, therefore $c_n(z = 0, r) = 0$ for $n \neq \pm 1$. Equation (1) was integrated in finite differences using the method of fractional steps and an operator-splitting procedure described in detail in several previous publications (Filonenko and Khokhlova 2001, Khokhlova et al. 2006, Canney et al. 2008).

Contrary to the previously developed algorithm, the nonlinear term in Eq. (1) was calculated here in the time-domain using a Godunov-type shock capturing method (Kurganov and Tadmor 2000,Bessonova et al. 2009). This algorithm can be used to simulate the propagation of nonlinear diffractive beams using only 6–8 temporal grid points at the shock front. The number of operations for modeling the nonlinear term in the time-domain is proportional to the number of temporal grid points (or harmonics), while in the frequency-domain simulations it is proportional to the square of the number of harmonics. Thus, if the time-domain is used for calculating the nonlinear substep, calculations can be accelerated while maintaining the same accuracy. The parameters of the numerical scheme were the same as described in the recent paper by Canney et al. (2008). The cylindrical grid had a radius of 45 mm and a length of 60 mm; Δz=0.1 mm and Δr=0.014 mm were the steps in the axial and radial directions, respectively; and the number of time points per fundamental acoustic period was 1024. To validate this newly developed part of the algorithm, the results of both codes were compared for the lowest and the highest values of the initial source output and never differed by more than 2%. Additional details on the methods used to set the boundary conditions for the model at $z = 0$ are provided in our recent publication (Canney et al. 2008).

The intensity of the wave was calculated using the results from the numerical solution of Eq. (1) as:

$$I(z,r)=f_0\int_0^{\frac{1}{f_0}}\frac{p^2(z,r,\tau)}{\rho_0 c_0}d\tau=\frac{1}{2\rho_0 c_0}\sum_{n=1}^{\infty}(4|c_n(z,r)|^2), \tag{3}$$

and included the intensities of all harmonics of the fundamental frequency generated through nonlinear propagation. Heat deposition due to absorption of ultrasound energy was obtained at each step in propagation distance, Δz, by accounting for the losses introduced at the absorption and nonlinear substeps in the operator-splitting procedure:

$$q(z,r)=-\frac{I(z+\Delta z,r)-I(z,r)}{\Delta z}. \tag{4}$$

The losses of acoustic energy due to absorption at the shocks were partially accounted for in the algorithm at the substep where the nonlinear term was calculated; therefore, both absorption and nonlinear (but not diffraction) substeps were included in calculating the heat deposition rate.

Heat transfer equation

The heat sources calculated using the results from the nonlinear acoustic “KZK” model, Eq. (4), were input into a heat transfer equation for calculating the temperature change in the gel and tissue samples

$$\frac{\partial T(r,z)}{\partial t}=k\nabla^2 T(r,z)+\frac{q(r,z)}{c_v}, \tag{5}$$

where T is the temperature in the medium, c_v is the specific heat capacity per unit volume, and k is the thermal diffusivity. Equation (5) was integrated numerically in finite differences using an explicit scheme with second order accuracy in both the time and spatial coordinates (Filonenko and Khokhlova 2001). The spatial windows of the cylindrical grid were 4.2 mm radially and 60 mm axially around the focus; the grid steps were Δz=0.1 mm and Δr=0.014 mm in the axial and radial directions, respectively; the temporal step was Δt=0.01 ms.

Calculations of focal intensity and heating

The peak focal values of the intensity and heating rate for the nonlinear acoustic model were calculated from Eqs. (3) and (4) and are labeled I_N and q_N. Besides numerical simulations of the nonlinear acoustic field, calculations were also performed assuming linear acoustic propagation by setting β=0 in Eq. (1); in this case, the peak intensity and heating rate are labeled I_L and q_L. In the linear case, the focal waveform is harmonic and Eq. (3) becomes

$$I_L=\frac{p_F^2}{2\rho_0 c_0}, \tag{6}$$

where p_F is the focal pressure amplitude, c_0 is the sound speed, and ρ_0 is the ambient density. The focal intensity, I_L, can also be estimated from linear simulations in water:

$$I_L \approx \frac{p_0^2}{2\rho_0 c_0} G^2 e^{-2\alpha_0 L}, \tag{7}$$

where p_0 is the **effective pressure amplitude** at the source, $G = p_F/p_0$ is the linear focusing gain of the source in water, α_0 is the absorption coefficient of the propagation medium at the source frequency, and L is the length in the axial direction of acoustic propagation to the focus in gel or tissue. Equation (7) provides a method for derating water measurements to tissue in the case of linear acoustic propagation.

The peak focal heating rate q_L calculated assuming linear acoustic propagation is proportional to the focal wave intensity, Eq. (6), and is given by

$$q_L=2\alpha_0 I_L. \tag{8}$$

Weak shock model of focal heating

When shocks are present in the focal waveform, an analytic expression based on weak shock theory (Hamilton and Blackstock 1998) can be used to estimate the peak heating rate:

$$q_{N,S}=\frac{\beta f_0 A_s^3}{6c_0^4\rho_0^2}, \tag{9}$$

where $q_{N,S}$ is the focal heating due to absorption at the shocks and A_s is the shock amplitude. Equation (9) was used to calculate the heating rate at output levels where shocks were present at the focus. The shock amplitudes, A_s, were obtained from the focal waveforms modeled numerically using Eq. (1) as well as measured using the fiber optic probe hydrophone (FOPH).

A shock wave is here defined as the waveform that exists when any slope of the modeled or measured pressure waveforms has a rise time on the order of the temporal grid step used in simulations, or the time scale limited by the bandwidth of the hydrophone in the measurements. Theoretically, the Taylor shock thickness or the rise time of a shock in a thermoviscous medium can be estimated from the stationary shock wave solution to the Burgers equation (Hamilton and Blackstock 1998, Cleveland et al. 2007). In a medium with a thermoviscous absorption equal to that of water, the theoretical rise time of shock waves with amplitudes of 40–80 MPa (measured and modeled in the work herein) is on the order of 0.1 ns. In the measurements, the bandwidth of the FOPH limited the rise time of shock wave measurements to 10 ns. The shock amplitude, A_s, in the measurements therefore was determined as the pressure change within 10 ns at the steepest part in the waveform. In the numerical code, shocks were resolved with 5–6 temporal grid steps of 0.5 ns, so the rise time was limited to 3 ns and defined within this width.

Estimations of additional heating due to shocks

When shocks form, the heating rates increase significantly. Consider here the excess heating $q_{N,S}$ due to the presence of shocks *versus* linearly predicted heating q_L over the range f focal intensities up to I_L = 25,000 W/cm^2 used in this study. In our previous paper, shock waves were measured in gel for linearly calculated focal intensities, I_L, higher than 6,000 W/cm^2 or focal pressure amplitudes, p_F in Eq. (6), higher than 14 MPa (Canney et al. 2008). The focal pressure amplitude p_F,Eq. (6), in the gel changes from 14 to 28 MPa over the interval of I_L from 6,000 to 25,000 W/cm^2. When the waveform was shocked, the peak positive pressure ranged from 40–80 MPa and was 3 times higher than the linearly predicted peak focal pressure, p_F. If we assume that the peak positive pressure is the shock amplitude, then the focal value of A_s in Eq. (9) can be calculated as $A_s = 3p_F$ (Canney et al. 2008,Bessonova et al. 2009). Then comparison of Eq. (9) using A_s to Eq. (8) using p_F yields $q_{N,S}$ from 40 to 83 times greater than q_L in gel over the range of output levels used in this study. In liver, where absorption α=0.7 dB/cm/MHz is higher, $q_{N,S}$ is 8 to 16 times greater than q_L over the same range of outputs. Since heat deposition due to shocks dominates the heating due to absorption of the fundamental frequency, Eq. (9) can be used as a good approximation of the focal heating both in gel and in liver when shocks are present.

Analytic estimation of time to boil

The peak focal heating rate was calculated using the three methods described above: using the numerically modeled focal heating, Eq. (4), using the weak shock model, Eq. (9), and using the heating predicted under assumption of linear wave propagation, Eq. (8). Then the temperature rise was calculated from the heating rates obtained with these three models. It is hypothesized that the heating can be sufficiently fast that thermal diffusion can be neglected in Eq. (5) and the time to boil, t_b, can be calculated analytically using only the peak focal heating rate as

$$t_b = \frac{\Delta T c_v}{q_F}, \tag{10}$$

where $\Delta T = 80°C$ and is the difference between the ambient and assumed boiling temperature of 100°C. The peak focal heating rate q_F was calculated using either the nonlinear model, Eq. (4); the linear model, Eq. (8); or, the weak shock estimate, Eq. (9).

The effect of thermal diffusion for the experimental conditions of this paper can be estimated from analytic solutions to Eq. (5). If the temperature distribution is assumed to have cylindrical symmetry with an initially Gaussian distribution of temperature, $T(t = 0, r) = T_0 \cdot e^{-r^2}/a^2$, then the analytic solution of Eq. (5) has the form (Morse and Feshbach 1953):

$$T(t,r)=\frac{T_0}{(1+4kt/a^2)}\cdot e^{-r^2/a^2(1+4kt/a^2)}. \tag{11}$$

Here, T_0 is the peak temperature, a is the initial radius of the heated region, and $k=1.3\times10^{-7}\text{m}^2/\text{s}$. The characteristic diffusion time, t_d, determined when the initial size of the heated spot increases by a factor of the square root of two, is

$$t_d=a^2/4k. \tag{12}$$

The radius of heat deposition within the focal volume of the HIFU transducer used in this paper, measured at the level of e^{-1} of its maximum, was 0.4 mm in the case of linearly predicted heating, thus the characteristic diffusion time in the gel given by Eq. (12) is 300 ms. At higher output levels, the excess heating due to the presence of shocks is much more localized: the radius of the focal heated spot is 0.1 mm (see Results section below), which gives a characteristic diffusion time of 19 ms. If the heating rate is so high that boiling starts in several milliseconds, then diffusion has little effect, and the time required to heat the sample to 100° C can be calculated using Eq. (10) with good accuracy.

Physical parameters used in modeling

The physical parameters used for modeling in water were $\rho_0 = 1000\ \text{kg/m}^3$, $c_0 = 1486$ m/s, and $\beta = 3.5$. The focusing gain of the transducer in water was determined from modeling and measurement as $G = 47.5$ (Canney et al. 2008). In the polyacrylamide gel phantom, the constants were $\rho_0 = 1044\ \text{kg/m}^3$, $c_0 = 1544$ m/s, $\beta = 4.0$, $c_v=5.3\times10^6\ \text{J m}^{-3}\ °\text{C}^{-1}$, and $k = 1.3\times10^{-7}\text{m}^2/\text{s}$, $\alpha_0 = 3.45\ \text{m}^{-1}$ at 2.158 MHz (0.15 dB/cm/MHz) (Lafon et al. 2005). For modeling in liver, the only physical parameter that was changed from simulations in water was the absorption, which was much higher, $\alpha_0 = 18.4\ \text{m}^{-1}$ at 2.158 MHz (0.70 dB/cm/MHz). The value of the absorption parameter in liver samples was obtained from measurements and, like the absorption in gel, was assumed to have a linear dependence with frequency. The axial path to the focus was water followed by 33 mm in gel phantom and either 27 mm or 13.5 mm in liver. The initial equilibrium temperature of the gel and liver was 20°C.

Experiments

The experimental arrangement is shown in Fig. 1. The ultrasound source was a single element, spherically focused piezoceramic crystal (PZ 26, Ferroperm Piezoceramics, Denmark) with a resonant frequency of 2.158 MHz that was air-backed and mounted in a custom-designed brass housing. The transducer had a 44-mm aperture and radius of curvature and was characterized in a previous study (Canney et al. 2008). The transducer was driven by a function generator (Model 33250A, Agilent, Palo Alto, CA) and a linear rf amplifier (55 dB gain, Model A300, ENI, Rochester, NY). The drive voltage at the transducer was monitored during experiments with a high-voltage probe. The pressure amplitude at the face of the transducer, p_0, was assumed to be proportional to the driving voltage as was measured and reported in our previous work

(Canney et al. 2008). Also, fluctuations in the voltage were used as a detector of boiling, as have been reported by others (Thomas et al. 2006,Khokhlova et al. 2009,Crum and Law 1995). A passive cavitation detector (PCD) was confocally aligned with the HIFU focus and consisted of a focused, 20-MHz transducer (0.75″ diameter, 2″ focal length, Harrisonics, Stamford, CT). The signal from the PCD was filtered using a 15-MHz high pass filter (Allen Avionics, Mineola, NY), preamplified (Model 5072PR, Panametrics, Waltham, MA), and recorded by a digital oscilloscope (Model LT342, Lecroy, Chestnut Ridge, NY). The PCD and HIFU drive voltage were not recorded continuously because of the limited memory of the oscilloscope. Instead, shorter sequences of points were recorded at a fixed pulse repetition frequency (PRF). Typically, 2000 data points sampled at 100 Megasamples/s were collected at a fixed repetition rate for the duration of HIFU heating. The PRF was chosen to maximize the usage of the onboard scope memory, which was limited to 1 million samples per channel. The acquired PCD and HIFU voltage signals were further processed in MATLAB (The Mathworks Inc., Natick, MA) and are displayed as either spectrograms or as the root mean squared (RMS) amplitude of the time series data.

Two different high-speed video cameras were used for filming experiments in the transparent gel phantom. In the first set of experiments, a Redlake M1 camera (color, Redlake, Tucson, AZ), filming at 1,000 frames per second with a resolution of 640 by 480 pixels was used. In the second set of experiments, a Photron Fastrax APX-RS camera (monochrome, Photron, San Diego, CA) was used and operated at 20,000 frames per second with a resolution of 512 by 256 pixels. A Nikon 105 mm lens (Nikon, USA) was used with a bellows extension for close-up photographs and provided a resolution of ~10 μm/pixel, which restricted the resolution of cavitation bubbles in the images. All experiments were backlit. The timing and triggering of the function generator for HIFU excitation, the oscilloscope for drive voltage and PCD signal acquisition, and the camera was performed by a timing board (NI 6608, National Instruments, Austin, TX), which was controlled by a custom acquisition program (Labview, National Instruments, Austin, TX).

All of the experiments were performed in a large acrylic water tank at room temperature (20° C). The water was purified using a reverse osmosis system and was degassed prior to measurements using a pin-hole degassing system to limit cavitation (Kaiser et al. 1995). The gas content of the water was measured using a dissolved oxygen meter (WTW Oxi 330i, Weilheim, Germany) and was less than 25% of saturation during all experiments. Both the PCD and the HIFU transducers were attached to a manual positioning system that allowed for them to be confocally aligned and moved vertically within the tank. The high-speed camera was also positioned using a lab jack. This arrangement allowed for HIFU exposures in up to 10 independent spots, separated vertically by 5 mm in a single gel or tissue sample. Since the camera was not used in the experiments in tissue, a second column of treatments could be made in tissue allowing for up to 20 separate exposures in each liver sample.

Tissue-mimicking phantom

The tissue-mimicking phantom used for the experiments has been used in several studies of HIFU dosimetry and consists of a polyacrylamide hydrogel with bovine serum albumen (BSA) added to increase the acoustic absorption of the gel (Chen et al. 2002, Khokhlova et al. 2006). In addition, the BSA serves as a temperature sensitive indicator; when the gels are heated above ~60°, the BSA protein denatures and turns opaque, allowing for visual observation of the region heated by HIFU. The phantoms used in the studies herein had a 7% w/v acrylamide concentration and 7% w/v BSA (Lafon et al. 2005). To prepare the tissue phantoms, the liquid mixture was first degassed for over an hour in a desiccant chamber and then poured into a custom gel phantom mold, where a polymerization agent was added. The gel phantom mold

was 5-cm wide (transverse to HIFU acoustic axis), 6-cm long (along HIFU acoustic axis), and 13-cm tall.

Measurements of the acoustic field were performed in the gel phantom prior to heating experiments using a fiber optic probe hydrophone (FOPH 2000, RP Acoustics, Germany) over a range of source drive levels up to p_0=0.57 MPa. For waveform measurements, the HIFU source was driven with a 30-cycle burst at a PRF of 10 Hz to limit heating and cavitation activity in the phantom during measurements. To calibrate the hydrophone for use in the gel phantom, the techniques described in a previous publication were used (Canney et al. 2008).

Ex vivo liver

The experiments with excised bovine liver samples were performed over four separate days using fresh liver tissue on each day. The liver was obtained from a local abattoir (Schenk Packing, Stanwood, WA) on the same day as the experiments and used within 12 hours. The liver was stored on ice and in a solution of phosphate buffered saline (PBS) until just before experiments were performed. The liver samples were prepared by cutting the liver into 8-cm wide by 8-cm tall by 2.7-cm thick pieces to fit a custom-designed tissue sample holder and an effort was made to avoid the presence of large vessels in the samples. Subsequently, the samples were degassed in a desiccant chamber for an hour and brought to room temperature (20°C) before being placed in the water tank for experiments. The external surface of the liver, the capsule, was maintained on one side of each sample and was oriented towards the HIFU source. The HIFU and PCD transducers were focused on an untreated spot in the tissue sample for each experiment.

In the first set of experiments with liver tissue, the FOPH was used to measure high amplitude focal waveforms after propagation through the 2.7-cm thick sample. The waveforms were measured in water behind the tissue sample at the spatial maximum of the peak positive pressure. The FOPH sensing tip was maintained in the water as opposed to implanted in the tissue due to the sensitivity of the calibration of the device to the properties of the surrounding medium. With this arrangement, there was less than 1 mm between the FOPH tip and the distal end of the tissue. Note that most of the high amplitude focal zone was therefore inside the tissue since the −6 dB axial length of the pressure distribution assuming linear acoustic propagation was 6.5 mm. To investigate the effect of the lump attenuation in the tissue sample, the focal waveforms measured in the presence of the sample were compared to measurements where the propagation was entirely in water. The waveforms from the tissue experiments were matched to those from the free field water measurements performed at lower outputs to account for attenuation during the propagation in tissue.

In addition to waveform measurements behind the liver sample with the FOPH at high output levels, the attenuation of the liver sample was also measured in a separate experiment using a transmission substitution technique. These measurements were performed at lower output levels with a more sensitive hydrophone [model GL-150-1A with 150-μm active diameter, Specialty Engineering Associates (SEA), Soquel, CA]. The HIFU source was operated without the rf amplifier using the function generator only and the amplitude of the focal waveform with the liver sample and without (water path only) was measured. At these low drive levels, the peak focal pressure was less than 1 MPa and the focal waveform was not distorted by nonlinear propagation effects. Comparison of the amplitudes of the focal waveforms with the liver sample in the propagation path and with a propagation path of water only were used to obtain the attenuation coefficient of the liver sample at the source drive frequency of 2.158 MHz.

After pressure measurements with the FOPH and SEA hydrophones, the HIFU focus was placed at a depth of 13.5+/−2 mm in the liver and the driving voltage to the HIFU source and PCD signals were monitored during heating. Liver samples were then exposed to HIFU at three

separate source output levels of p_0=0.42 MPa, 0.49 MPa, and 0.57 MPa and the time to boil was measured using the PCD and HIFU drive voltage signals.

Body wall (inhomogeneous tissue path)

In clinical studies, the acoustic propagation path is more complex than in tissue phantoms and contains both multiple tissue layers (each with different densities and sound speeds) as well as smaller-scale inhomogeneities within each layer. Since the acoustic properties are not uniform throughout the acoustic path in such situations, the focusing of the source may become degraded due to refraction, phase aberration, and scattering, resulting in a loss of focusing gain and therefore reduced nonlinear effects at the focus for a given output level. These effects have been investigated previously in diagnostic imaging since the presence of multiple tissue layers can degrade the quality of images (Mast et al. 1997). To address these concerns in the context of the present study and to demonstrate whether shock waves form in inhomogeneous tissue, experiments were performed using a sample of porcine body wall. The tissue sample was harvested after separate IACUC approved experiments and euthanasia according to the university IACUC rules. The harvested sample was 2-cm thick and approximately 10-cm square and was transferred to the water tank for experiments within an hour after the tissue was harvested. The outer surface of the body wall (skin) was oriented towards the HIFU source. After the body wall was positioned in the water tank, waveform measurements were performed less than 1 mm from the tissue distal surface at the focus of the HIFU source using the FOPH.

Results

Acoustic field measurement and modeling in tissue phantoms

Results of measurements and simulations of the acoustic field in gel at HIFU drive levels of p_0=0.048 MPa (I_L=144 W/cm^2, I_N =145 W/cm^2) and p_0=0.44 MPa (I_L= 12,000 W/cm^2, I_N =16,700 W/cm^2) are shown in Fig. 2. The focal waveforms measured using the FOPH and modeled are plotted in Fig. 2a for both output levels. At the lower output, the wave is nearly sinusoidal—peak positive pressure is 2.2 MPa and peak negative is 2.0 MPa—and is considered linear. The agreement between the simulated and measured waveforms is excellent. At the higher output, the wave is shocked and the measured and simulated waveforms still agree very well. However, the measured peak positive pressure is lower than the simulated value, which is due to incomplete correction of the limited bandwidth of the FOPH hydrophone. Evidence was presented in Canney et al. (2008) that the modeled waveforms were more accurate than measurements when shocks were present. The accuracy of the model is tested further throughout this section.

Figures 2b and 2c show two-dimensional axial distributions of the peak positive and peak negative pressures, intensity I, and heating rate q calculated using the nonlinear model, Eq. (1). The contour plots depict the −1 dB, −3 dB, and −6 dB region in the distributions of each acoustic variable. In the low-amplitude, linear case (Fig. 2b), the contours are constant across all parameters and in the high amplitude, nonlinear case (Fig. 2c), the contours are different for each field parameter.

At the lower output level, the spatial distributions of the peak positive and peak negative pressure are the same, as well as the distributions for the intensity and the heating. The intensity and heating rate are proportional to the square of the pressure amplitude, Eq. (6), and are linearly related by a factor of $2\alpha_0$ to each other, Eq. (8). The distributions of the pressures, intensity, and heating are nearly equivalent at this output level; therefore, only one field variable can be used to describe all of the acoustic quantities of interest.

At the upper output level of p_0=0.44 MPa, the spatial distributions of acoustic field parameters vary for each parameter. The dimensions of the focal region of the peak positive pressure become significantly smaller. The heated region shrinks even more. Increasing from the lower output to the higher output, the −6 dB width of the positive pressure changes from 1 mm to 0.4 mm and that of the heating rate from 1 mm to 0.20 mm. The narrowing of the intensity field is less pronounced and changes from 1 mm to 0.8 mm. The distribution of the peak negative pressure, contrary to the peak positive pressure, intensity, and heating, becomes wider and changes from 1 mm to 1.2 mm, with the maximum shifted toward the transducer. The variation in spatial distributions shown in Fig. 2c makes it clear that the relationship among field variables is not as simple as it was for the linear case. In short, the peak positive and negative pressures are not equal in nonlinear HIFU fields and the heat deposition is not proportional to the *in situ* intensity. Instead, the heating and intensity are related by the product of the frequency-dependent absorption and the intensity at each frequency present in the wave as shown in Eq. (4).

Figure 3 depicts the peak focal heating rates in gel calculated over a range of source output levels from p_0=0.048 MPa (I_L =144 W/cm^2, I_N = 145 W/cm^2) to p_0=0.57 MPa (I_L=20,000 W/cm^2, I_N = 25,500 W/cm^2) using the four different methods described in the Theory Section. The curve labeled “Linear Model” corresponds to calculations using Eq. (8). The curve labeled “Nonlinear Model” corresponds to calculations of the heating rate using Eq. (4). The last two curves correspond to calculations using weak shock theory, Eq. (9). The shock amplitudes for the curves based on weak shock theory, “Weak Shock (FOPH)” and “Weak Shock (KZK)”, were obtained from either the measured or modeled focal waveforms when shocks were present. The modeled focal waveforms are shown on the top of the figures to illustrate how the heating rates are related to the waveforms.

At lower source outputs (p_0<0.24 MPa, I_L<3,700 W/cm^2, I_N <4,200 W/cm^2), the focal waveforms are already distorted but not yet shocked. A moderate increase in focal heating relative to the linearly predicted heating results from the nonlinear generation and absorption of the higher harmonics. When a shock starts to develop at the focus (p_0 =0.30 MPa, I_L =5,800 W/cm^2, I_N =7,000 W/cm^2), the heat deposition rate calculated using full nonlinear modeling increases dramatically over linear predictions. When a shock is formed at the focus (p_0=0.34 MPa, I_L=7,300 W/cm^2, I_N =9,600 W/cm^2), the heating rate calculated using the nonlinear model is 50 times higher than the heating calculated assuming linear propagation. The difference between the nonlinearly and linearly calculated heating increases to 83 times at the highest excitation level of p_0=0.57 MPa.

The results of calculations using weak shock theory and the shock amplitude from the measured waveform, “Weak Shock (FOPH)”, yield lower heating than in the full nonlinear modeling because the peak positive pressure and thus the shock amplitude itself is underestimated in the measurements. However, the heating rate calculated using weak shock theory and the shock amplitude obtained from the modeled waveform, “Weak Shock (KZK)”, agrees very well with results of the numerical “Nonlinear Model”.

Measurement and modeling of millisecond boiling in tissue phantoms

Following measurement and modeling of acoustic field parameters in a tissue phantom, heating experiments were performed to measure the time to initiate boiling in the phantoms. In Fig. 4, a sequence of high-speed video frames is shown during 9 ms of heating at an output level of p_0=0.44 MPa (I_L=12,000 W/cm^2, I_N =16,700 W/cm^2). The HIFU source was located on the left side of the images. The needle in the top right corner of each frame was used for aligning the camera with the HIFU focus. The tip of the needle coincides with the axial position of the HIFU focus, but is 3 mm above the focus. The results of numerical modeling of the acoustic field are also overlaid on the high-speed image in Fig. 4a and show the size and position of the

frame relative to the HIFU source. The frame extends from 37.5 mm to 46.5 mm in the axial direction and from −3.5 mm to 3.5 mm in the radial direction. The peak pressure at this output level is located on the beam axis, r=0, at z=43 mm. The inner contour (dashed curve) in the plot depicts the −6 dB region of the peak positive pressure. The contour levels for 3 MPa and 6 MPa peak negative pressures are also shown in the plot (solid curves) and correspond to the minimum and maximum cavitation thresholds measured in the tissue-mimicking phantom (Khokhlova et al. 2009).

In the first frame (Fig. 4a), which was recorded after 1 ms of heating, small cavitation bubbles are observed throughout the frame in the region within the outer contour (which corresponds to peak negative pressures of greater than 3 MPa). Cavitation bubbles are seen moving through the gel in the high-speed movies, presumably pushed by acoustic radiation force. This movement is observed in the high-speed image by the presence of long (1–2 mm) tracks behind the bubbles. Within the first several milliseconds, all of the observable bubbles were quickly pushed out of the region of highest pressure (corresponding to the dashed inner contour) and are only visible outside the region of the highest peak positive pressure. After 5 ms of heating (Fig. 4b), a darkened region can be seen corresponding to the dimensions of the dashed contour. This darkened region was likely caused by optical changes of the gel phantom as it was heated, but was not caused by denaturing of the BSA protein, since it was reversible and disappeared when the gel phantom cooled back to ambient temperatures after HIFU heating. After 9 ms of heating (Fig. 4c), a large boiling bubble appeared suddenly and filled the region corresponding to the −6 dB of peak positive pressure, which also coincides spatially with the highest shock amplitude and thus the highest heating rate. The large boiling bubble persisted throughout the remainder of heating (150 ms in this experiment), grew in size, and moved towards the transducer.

Figure 5 shows two sequences of high-speed video frames (20,000 fps) at various time points during two separate exposures in which a gel phantom was heated for 4.8 ms at the highest output level of p_0=0.57 MPa (I_L=20,000 W/cm^2, I_N =25,500 W/cm^2) used in this study. These frames are cropped to only show the region where boiling onset occurs and are 4.4 mm in length axially and 2.2 mm in width around the focus. In the first exposures, Fig. 5a, a growing boiling bubble is observed that is formed from three smaller nuclei visible in the main focal volume in the previous frame at 3.85 ms. Subsequently, the three bubbles coalesce into one larger boiling bubble (1 mm long by 0.5 mm wide), which was present in the same position of the focal lobe until the HIFU was turned off at 4.8 ms. When the HIFU is turned off, interestingly, visible bubbles, cavitation or boiling, grow in the first frame and only the first frame following HIFU stopping. Then cavitation bubbles disappear from view, and the boiling bubble remains quiescently slowly shrinking over a period of at least several seconds. We speculate that non-condensable gas from the incompletely degassed gel diffuses into the bubble during boiling and that the bubble persists as this gas re-dissolves into the gel. In the second exposures, Fig. 5b, where no bubble nuclei were visible, boiling onset took slightly longer, and resulted in 4.25 ms. Thus, it is likely that the nucleus for boiling was smaller in Fig. 5b and thus greater amounts of superheat were necessary to initiate explosive boiling bubble growth (Plesset and Zwick 1954).

Simultaneously during filming the heating of gel and onset of boiling, acoustic signals from the focal region were detected using a PCD. In the PCD signals, there is a clear distinction between cavitation and boiling activity that corresponds to the visual observations made with the high-speed camera. Figure 6 shows both high-speed video and PCD data for two different experimental exposure levels—p_0=0.34 MPa (I_L=7,300 W/cm^2, I_N = 9,600 W/cm^2) for 500 ms of HIFU exposure and p_0=0.57 MPa (I_L=20,000 W/cm^2, I_N = 25,500 W/cm^2) for 30 ms of HIFU exposure in gel phantoms. The plots on the left side show the time-domain and

spectrogram representations of the recorded PCD signal. The high-speed images on the right show frames at selected time points during heating.

In the lower power heating experiment (p_0=0.34 MPa) the visual appearance of boiling correlates with distinct signatures in the PCD data. First, in the video frame after 130 ms, a thermal lesion, caused by denaturing of the BSA protein in the gel, appeared. The signal that appears in the PCD data at 130 ms is attributed to cavitation and was not well correlated with the timing of lesion formation. After 240 ms, a large millimeter-sized bubble suddenly appeared and persisted pulsating with amplitude on the order of its radius until the HIFU ceased at 500 ms. Simultaneously at 240 ms, the volts-vs-time representation of the PCD data showed a spike in amplitude that generally persisted: the bubble grows and pops so violently particularly at first that sometimes it jumps out of the PCD focal region. Also at 240 ms, the frequency-vs-time spectrogram of the PCD data shows a change. The signal becomes noticeably larger and covers more of the frequency range shown in the plots. This spectrogram appearance is largely a reflection simply of the stronger signal. However, the spectrogram also takes a signature of bands of horizontal stripes. These stripes are the result of high signal content at the harmonics of the HIFU fundamental frequency. Specifically, the bandwidth of the PCD encompasses the 7th (15.1 MHz) through the 13th (28 MHz) harmonics of the 2.158 MHz HIFU fundamental. We speculate this signature is the result of the shocked HIFU wave (which contains multiple harmonics) largely reflecting from the bubble to the PCD. This is consistent with the interpretation by others (Farny et al. 2008). As the thermally driven boiling bubble is distinct in appearance from the mechanically driven cavitation bubbles (apparent in Fig. 4), the boiling and cavitation signatures are distinct in the PCD signals. On the volts-vs-time trace, cavitation is the very low level signal before boiling. In the spectrogram, cavitation creates the fairly uniform signal on the spectrogram between 15 MHz and 22 MHz. The uniformity indicates broadband noise, which is consistent with short duration pressure spikes emitted during inertial cavitation bubble collapse (Leighton 1994).

At the higher output level (p_0=0.57 MPa) cavitation and boiling have the same appearance as at the lower level but occur faster. The cavitation signature is seen from time zero in the PCD plots and lessens slightly over a few ms. At 4 ms, a boiling bubble appears in the camera frame, and the boiling signatures are seen on the PCD traces. The boiling bubble and PCD signatures remain until HIFU ceases at 30 ms. Note, no thermal lesion was observed in the video images before boiling occurred. We speculate that the heating is too fast for the protein to denature.

The drive voltage at the HIFU transducer was also monitored during the experiments described above. At the same time boiling was detected by the PCD and high-speed camera (note the acoustic time delay from the bubble to the PCD or HIFU source should be taken into account but is much shorter than 1 ms), the RMS voltage to the HIFU source fluctuated by approximately 5%. The signals appear similar to the figure in the Liver Results Section. The fluctuation in voltage has previously been attributed to the transduction of the change in acoustic impedance caused by the appearance of the large, millimeter-sized boiling bubble (Crum and Law 1995, Khokhlova et al. 2009, Thomas et al. 2006). No fluctuation was present when cavitation was observed with the other methods, arguably simply because the impedance change from cavitation was weaker than detected by the method as we employed it. However, voltage fluctuation, PCD, and high-speed camera each clearly showed the onset of boiling at the same time.

Figure 7 summarizes the time to boiling obtained in high-speed filming experiments when the focal waveform in the HIFU field was shocked. The focal waveforms are shown at the top of the figure for the lowest and highest output levels where shocks were present in experiments. The measured peak pressures ranged from 41 MPa to 63 MPa and were lower than calculations, which ranged from 57 MPa to 79 MPa. At the bottom of the figure, the mean measured times

to boiling onset plus and minus one standard deviation are plotted *versus* HIFU source pressure. The times to boiling are between 52 ms at the lowest output and 4 ms at the highest (note that 4 ms is only 8000 acoustic periods at 2 MHz). Small changes in the initial pressure thus cause large changes in the heating rate and corresponding time to boil, especially in the transition to pressures where shock waves just begin to form.

Also plotted in Fig. 7 are the results of four separate calculations of the time to reach 100°C. The solid line shows the calculation with the full nonlinear model of acoustic and temperature fields, Eqs. (1) and (5). The large dashed line came from the same model but with the thermal diffusion term in Eq. (5) neglected. The other two lines were calculated analytically based on weak shock theory, Eq. (9), and focal shocked waveforms. In one curve, the waveform calculated with the KZK nonlinear modeling was used to obtain the shock amplitude, A_s. In the other curve, the waveform measured with the FOPH was used to estimate the shock amplitude. Calculations with the full nonlinear modeling and those with weak shock theory and the KZK-simulated waves are in excellent agreement with the measurements. The analytic estimates from the FOPH-measured waveforms and weak shock theory produced longer times to boil because the shock amplitudes are lower in measurements than those obtained in simulations with the nonlinear model. Nevertheless, all the times to boil, measured and calculated, show the same nonlinear response and also produce boiling in only milliseconds. All the data taken together show that these HIFU exposures, which are within the clinical range of frequency, gain, and electrical power, yielded boiling in milliseconds. The estimate of time to boil obtained from modeling was closer to the experimentally observed initiation of boiling using the high-speed camera, which supports the hypothesis that the modeled waveforms are more accurate than the measured ones.

The time to boiling is not shown for the linear model neglecting diffusion, Eq. (8). These values are from 770 ms to 320 ms over the range of outputs shown in Fig. 7 and are thus off the scale of the plot and orders of magnitude slower than what was measured. In addition, when thermal diffusion is included, these times are even slower as thermal diffusion makes slower heating even slower and has little effect on faster heating. This is observed in the discrepancy at the lowest output level of p_0=0.37 MPa where predictions which neglect thermal diffusion yield faster initiation of boiling than either those that include diffusion or experimental results. The time where this underestimation occurs (>20 ms) correlates well with the characteristic diffusion time of 19 ms calculated in the Theory Section. When boiling occurs in times longer than the diffusion time, heat is lost due to diffusion and the peak temperature rise is slowed. But for faster heating, thermal diffusion is insignificant and does not effect the peak temperatures generated during HIFU heating.

Acoustic field measurements in liver tissue

Figure 8a shows a photograph of the arrangement used to measure focal waveforms behind liver tissue. The curve labeled “FOPH (Liver)” in Fig. 8b shows the focal waveform measured behind the liver sample with the fiber optic hydrophone at an output level of p_0=0.49 MPa. The waveform is shocked with a peak positive pressure of 45 MPa and peak negative pressure of 11 MPa. Since liver tissue is much more absorptive than water, the peak pressure values here were smaller than when the propagation path was in water only. The focal waveform in free-field water measurements at the same output was shocked with a peak positive pressure of 65 MPa and peak negative pressure of 15 MPa (Canney et al. 2008).

Also shown in Fig. 8b is a waveform measured in water with the FOPH at a lower source pressure. The free-field water measurement, “FOPH (Water)”, yields a very similar waveform shape and peak pressure as the waveform measured behind the liver sample. To attain the agreement in the measured focal waveforms, the source pressure was scaled using the relation

$$p_0(water)=p_0(liver)\cdot exp(-\alpha_0 L), \quad (13)$$

where α_0 is the unknown lumped attenuation over the tissue path of thickness L. The waveforms measured in water for an initial pressure of p_0=0.29 MPa agree well with the measurements for p_0=0.49 MPa, which yields overall losses of 4.3 dB in the pressure amplitude. The attenuation coefficient α_0 is then equal to 1.6 dB/cm at the source frequency of 2.158 MHz or 0.7 dB/(cm MHz) if the attenuation is assumed to have a linear dependence with frequency. This result agrees well with the value of 1.6 dB/cm obtained for the same piece of tissue by comparing low amplitude waveforms measured with and without the liver present as described in the Methods Section; it is also within the range of attenuation values in liver of 0.35–0.7 dB/(cm MHz) reported in other studies (Duck 1990).

Lastly, modeling was performed using Eq. (1) to simulate the focal waveform in liver using an attenuation of α_0=1.6 dB/cm. This curve is shown in Fig. 8b as "KZK (Liver)". The rest of the acoustic properties of liver in simulations were assumed to be the same as in water. The focal waveform obtained in modeling is also in excellent agreement with both measurement results.

The agreement between the high amplitude focal waveforms observed using Eq. (13) to match output levels in water and tissue suggests a new derating approach for HIFU. The new approach involves comparing nonlinear HIFU fields in water and in tissue not for the same source output, as is usually done in the existing derating techniques, but for the same focal pressures equalized by scaling the source outputs. The method can be used to estimate the focal waveform in tissue since in HIFU, high gain sources are typically used and nonlinear effects are much more significant in the focal region than elsewhere. The losses in tissue over the lower amplitude path to the focus are then well approximated by using only the attenuation at the source frequency. When the source pressures are scaled to account for linear attenuation losses in tissue, then both the pressure levels at the focus as well as the degree of nonlinear waveform distortion should be similar in water and in tissue. However, even if α_0 is not known, rapid boiling might be induced to attain the attenuation. If the time to boil is determined and is sufficiently fast to neglect thermal diffusion, then the *in situ* shock amplitude can be determined using Eqs. (9) and (10). From comparison of the *in situ* shock amplitude to those determined in water, Eq. (13) can be used to estimate the attenuation α_0.

Figure 9 shows focal waveforms simulated both in liver at a depth L of 13.5 mm (solid lines) and in water (dashed lines) at three different output levels. The waveforms are shifted in time in the plot for visual convenience. The output levels for direct simulations in liver were p_0=0.42, 0.49, and 0.57 MPa and yield peak positive pressures of 48.5, 58.8, and 66.6 MPa in the focal waveforms. For simulations in water, the source pressure outputs were chosen 22% lower than those in liver according to the derating approach, Eq. (13), with α_0=1.6 dB/cm and L=13.5 mm. The peak positive pressures in these derated waveforms were slightly higher than those for the simulations in liver—52.2, 62.5, and 70.3 MPa; however, the shock amplitudes A_s in the corresponding waveforms in liver and in water are equal. The shock front as a whole is shifted slightly downward in the waveform in liver, which is typical for shocked waveforms developed in dispersive media (Kashcheeva et al. 2000).

Overall, the waveforms simulated directly in liver and derated from simulations in water are nearly identical; shock fronts are present in both waveforms and grow in amplitude as the source output level is increased. Similarity in the waveforms validates the proposed derating approach and these results demonstrate that a table of focal waveforms measured in water and

a measurement of the linear absorption value in tissue can be used to obtain nonlinear focal waveforms in tissue and to estimate nonlinear thermal effects due to shocks.

Boiling onset measurements in liver tissue

Figure 10 shows the HIFU drive voltage and PCD signals obtained during 40 ms of heating at an initial source pressure of p_0=0.49 MPa in liver tissue. An additional 10 ms was acquired prior to the start of HIFU to show the baseline signal levels for both sensors. The HIFU drive voltage and PCD signals both show a dramatic jump after 7.5 ms of heating. Consistent with our experience in gels, where the start of boiling could be visually observed, the simultaneous signatures on these two sensors are taken as indicative of boiling activity after 7.5 ms of heating. The small increase in PCD signal level at the start of HIFU consisted of broadband noise in the frequency domain similar to the signals recorded in gel phantoms and was likely due to cavitation activity.

Figure 11 presents a summary of heating experiments and modeling in *ex vivo* liver samples. The results are shown as means plus and minus standard deviations of time to boil obtained for three different source output levels p_0=0.42 MPa (I_L=8,400 W/cm^2, I_N =11,100 W/cm^2), 0.49 MPa (I_L=11,400 W/cm^2, I_N =15,200 W/cm^2), and 0.57 MPa (I_L=15,400 W/cm^2, I_N =20,100 W/cm^2). The *in situ* intensities here are focal intensities in the middle of the liver samples and are obtained from the results of modeling using Eqs. (3) and (6) and the attenuation value in liver determined above. The mean times to initiation of boiling were 38 ms at p_0=0.42 MPa, 10.4 ms at p_0=0.49 MPa, and 5.7 ms at p_0=0.57 MPa and were determined using the acoustic signatures similar to those shown in Fig. 10. In addition to the experimental data, the results of modeling of heating in liver are presented and calculated using three separate methods. The first calculation shows the results of simulations of temperature rise to 100°C using the nonlinear model when thermal diffusion was neglected. The second calculation shows the results of the nonlinear model with thermal diffusion included. The last result is the estimate based on weak shock theory and the shock amplitudes obtained from the waveforms simulated in liver shown in Fig. 9. It is found that when the time to boil is estimated assuming linear acoustic propagation without thermal diffusion using Eqs. (7), (8) and (10), then the boiling times are off the scale in Fig. 11 and are 137 ms at p_0=0.42 MPa, 100 ms at p_0=0.49 MPa, and 75 ms at p_0=0.57 MPa.

Waveform measurements in tissue body wall

Figure 12 shows a waveform measured through a 2-cm thick sample of excised porcine body wall as well as a photograph of the experimental arrangement. The HIFU source was operating at an output level of p_0=0.57 MPa and a shocked waveform with peak positive pressure of 24 MPa and peak negative pressure of 7 MPa was measured at the focus. The waveform measured behind the body wall agrees well with the waveform measured in water at an output level of p_0=0.25 MPa, which yields a lumped attenuation of 7.2 dB using the proposed derating method. However, the waveform measured in water has distorted but not yet shocked whereas the one in tissue has shocked: the rise of the pressure measured in the tissue is visibly steeper than the rise of the pressure measured in water. The difference is present but less noticeable at higher amplitude and in different tissue in Fig. 8. A plausible explanation is that the nonlinearity parameter β is higher in tissue, especially fat, than in water. Higher β leads to stronger nonlinear acoustic propagation distortion and earlier shock formation, thus shocks may form at a lower *in situ* focal pressure (alternatively focal intensity) in tissue than in water.

Discussion

The primary result from this study is that shock waves occur in tissue under clinically relevant exposures, accelerate heating by orders of magnitude over estimates assuming linear acoustic

propagation, and induce boiling in milliseconds. Heating rates are very sensitive to the source output level when shocks start to form at the focus, i.e. a small increase in source output can have a dramatic effect on heating. In this study, shocks formed in tissue phantoms near an *in situ* intensity of 6,000 W/cm^2. A change in output from a pre-shock level (p_0=0.29 MPa, I_L=5,400 W/cm^2) to one in which shocks formed (p_0=0.39 MPa, I_L=9,400 W/cm^2) resulted in a 20-fold increase in heating rates as compared to those predicted assuming linear propagation. This enhancement increased to a maximum of 83-fold in low absorptive tissue phantoms and 16-fold in liver and led to boiling in only several milliseconds in both cases. Furthermore, the enhanced heating was highly predictable in location and magnitude by using either numerical modeling or, when shocks were present, using an analytic solution based on weak shock theory. A method for predicting nonlinear HIFU fields and heating rates in tissue using either the results of measurements or modeling in water was presented. Experimental techniques to detect and separate boiling and cavitation activity during HIFU exposures were also demonstrated.

The experiments performed in this study have implications for the physical mechanisms of action of HIFU treatment. The high-speed movies obtained in transparent gel phantoms (Fig. 4) clearly distinguish thermally generated boiling bubbles from mechanically generated cavitation bubbles. Cavitation was visually observed immediately after HIFU was turned on by the formation of bubbles that were tens of microns in diameter distributed throughout the spatial region corresponding to negative pressures exceeding the cavitation threshold of the phantoms. Boiling occurred after only several milliseconds at the highest exposures, was localized at the focus, and was visible by the appearance of millimeter-sized bubbles. Although boiling bubbles were created thermally, at sufficient heating rates, no denaturing of the BSA protein in the gel was observed before the bubble formed and filled the focal region with a void of mechanical damage. Thus, the possibility exists that the thermally generated bubble results in predominantly mechanical damage; in other words, the highly predictable location and timing of boiling might be used to reliably generate tissue erosion as desired in histotripsy applications (Parsons et al. 2006) or for targeting HIFU treatments (Vaezy et al. 2001,Rabkin et al. 2006).

Boiling and cavitation activity can be distinguished in visual observations or acoustically using the 20-MHz PCD and by monitoring the drive voltage to the HIFU source. Significant fluctuations in the drive voltage were present only when boiling occurred, while the PCD was sensitive to both cavitation and boiling activity in the phantoms. In the PCD signals, broadband signals were detected immediately after HIFU was turned on, but quickly weakened in amplitude. The decrease in PCD signals may be due to a softening of bubble collapse due to elevated temperatures and therefore increased vapor in the bubbles (Kreider 2008) but the high-speed movies also show that in the gel, cavitation bubbles are quickly pushed out of the focal region due to radiation pressure. These observations demonstrate that the sensors are far more sensitive to boiling than cavitation. Furthermore, as we previously stated (Khokhlova et al. 2009), these observations led us to believe that shock wave enhanced heating had already been observed *in vivo* (Sokka et al. 2003) and misinterpreted as cavitation-enhanced heating. Although cavitation was observed during all of the experiments in our study, there was little evidence of additional heating due to cavitation bubbles since modeling of temperature rise to 100°C agreed well with the experimentally measured times to initiation of boiling in both tissue phantoms and liver. This study has made contributions to the use and understanding of these monitoring methods that are consistent with the observations of others (Thomas et al. 2006, Farny et al. 2008, Crum and Law 1995) and with our own observations that HIFU-induced boiling and not cavitation created clear echogenicity on B-mode ultrasound (Khokhlova et al. 2006).

Although the studies herein were not performed *in vivo*, even *in vitro* measurements are clinically relevant. The primary difference between *in vivo* and *in vitro* here is the distribution

of gas nuclei. Both cavitation and boiling rely on a seed or nucleus, and the distribution is not well-known. A sparse distribution of tiny nuclei would mean boiling occurs above 100°C as higher temperatures are required to overcome the higher surface tension of smaller bubbles (Plesset and Zwick 1954). We found a visible bubble in the focal region led to slightly earlier boiling (less heating and a lower temperature) than when a bubble was not visible. But variation in boiling times was rather small and 100°C was a reasonable approximation to when boiling occurred in the experiments. Another difference between *in vivo* and *in vitro* measurements is that perfusion is not present. In most HIFU studies, it is assumed that perfusion acts too slowly to affect heating over exposures that are only seconds in duration. In this study, it is demonstrated that in millisecond exposures and heating, not only perfusion, but thermal diffusion can be neglected as well.

Lastly, this study demonstrated both a direct numerical method and a novel derating method for determining both pressures and heating rates in nonlinear HIFU fields in tissue. The proposed derating method relies on scaling the source pressure amplitude, not focal pressure amplitude, between water and tissue measurements. Briefly, the focal waveform determined in water at the lower output level will correspond to the focal waveform in tissue at the higher output level scaled to account for the linearly calculated absorption in tissue. In the acoustic fields of the highly focused sources used in HIFU, nonlinear propagation effects are insignificant except in the high-amplitude focal region; therefore, losses in the path to the focus can be accounted for by a lumped attenuation coefficient at the source fundamental frequency and nonlinear propagation effects observed in water are similar to those in tissue. Thus, measurement or modeling of HIFU fields in water over the range of source outputs used for treatments, in combination with the attenuation of the tissue path, is sufficient for accurate prediction of both pressures and heating rates *in vivo*. Conversely, the measurement of millisecond boiling (at an output level where shocks are formed and thermal diffusion can be neglected) can be used to estimate *in situ* acoustic fields and attenuation.

Acknowledgments

The work at the Center for Industrial and Medical Ultrasound (CIMU) at the Applied Physics Laboratory has been supported by the National Space Biomedical Research Institute (SMST01601) in consortium agreement with the National Aeronautics and Space Administration and the National Institute of Health (DK43881 and EB007643). The work at Moscow State University has been supported by the Russian Foundation for Basic Research (09-02-00066 and 08-02-00368) and by the International Science and Technology Center (3691). The authors gratefully acknowledge the help of Brian MacConaghy, Andrew Proctor, and Fran Olson for help in the design and construction of the experimental setup. We are very thankful to Oleg Sapozhnikov and Wayne Kreider for fruitful discussions and to Mikhail Averianov for help with modifying the numerical code. We also wish to thank the staff and researchers at CIMU and at the Consortium for Shock Waves in Medicine (CSWM).

References

Bessonova O, Khokhlova V, Bailey M, Canney M, Crum L. Focusing of High Power Ultrasonic Beams and Limiting Values of Shock Wave Parameters. Acoust Phys 2009;55(4–5):445–456.

Canney M, Khokhlova V, Bailey M, Sapozhnikov O, Crum L. Acoustic characterization of high intensity focused ultrasound fields: A combined measurement and modeling approach. J Acoust Soc Am 2008;124(4):2406–2420. [PubMed: 19062878]

Chen W, Lafon C, Matula T, Vaezy S, Crum L. Mechanisms of Lesion Formation in High Intensity Focused Ultrasound Therapy. IEEE Ultrason Symposium 2002;2:8–11.

Clarke R, ter Haar G. Production of harmonics in vitro by high-intensity focused ultrasound. Ultrasound Med Biol 1999;25(9):1417–1424. [PubMed: 10626629]

Clement, G.; McDannold, N.; Hynynen, K., editors. Therapeutic Ultrasound: 5th International Symposium on Therapeutic Ultrasound. Boston, MA. October 27–29, 2005; AIP Conference Proceedings; 2005.

Cleveland R, Chitnis P, McClure S. Acoustic Field of a Ballistic Shock Wave Therapy Device. Ultrasound Med Biol 2007;33(8):1327–1335. [PubMed: 17467154]

Cleveland R, Lifshitz D, Connors B, Evan A, Willis L, Crum L. In vivo pressure measurements of lithotripsy shock waves in pigs. Ultrasound Med Biol 1998;24(2):293–306. [PubMed: 9550188]

Crum, L.; Law, W. The Relative Roles of Thermal and Nonthermal Effects in the use of High Intensity Focused Ultrasound for the Treatment of Benign Prostatic Hyperplasia. 15th International Congress on Acoustics. International Congress on Acoustics; Trondheim, Norway. June 26–30 1995; p. 315-318.

Dalecki D, Carstensen E, Parker K. Absorption of finite amplitude focused ultrasound. J Acoust Soc Am 1991;89(5):2435–2447. [PubMed: 1861004]

Duck D, Starritt H. Acoustic shock generation by ultrasonic imaging equipment. Br J Radiol 1984;57:231–240. [PubMed: 6697084]

Duck, F. Physical Properties of Tissue: A Comprehensive Reference Book. Academic Press; 1990.

Farny C, Holt R, Roy R. Temporal and Spatial Detection of HIFU-Induced Inertial and Hot-Vapor Cavitation with a Diagnostic Ultrasound System. Ultrasound Med Biol 2009;35(4):603–615. [PubMed: 19110368]

Filonenko E, Khokhlova V. Effect of Acoustic Nonlinearity on Heating of Biological Tissue by High-Intensity Focused Ultrasound. Acoust Phys 2001;47(4):541–549.

Hamilton, M.; Blackstock, D., editors. Nonlinear Acoustics. Academic Press; London: 1998. p. 105-106.

Hill, CR.; Bamber, JC.; ter Haar, G. Physical Principles of Medical Ultrasonics. 2. John Wiley & Sons; West Sussex, England: 2004.

Hynynen K. Demonstration of enhanced temperature elevation due to nonlinear propagation of focused ultrasound in dog's thigh in vivo. Ultrasound Med Biol 1987;13(2):85–91. [PubMed: 3590364]

Kaiser A, Cain C, Hwang E, Fowlkes J, Jeffers R. A cost effective degassing system for use in ultrasonic measurements: The multiple pinhole degassing system. J Acoust Soc Am 1995;99(6):3857–3860.

Kashcheeva S, Sapozhnikov O, Khokhlova V, Averkiou M, Crum L. Nonlinear distortion and attenuation of intense acoustic waves in lossy media obeying a frequency power law. Acoust Phys 2000;46(2): 211–219.

Kennedy J. High-intensity focused ultrasound in the treatment of solid tumours. Nat Rev Cancer 2005;5 (4):321–7. [PubMed: 15776004]

Khokhlova T, Canney M, Lee D, Marro K, Crum L, Khokhlova V, Bailey M. Magnetic resonance imaging of boiling induced by high intensity focused ultrasound. J Acoust Soc Am 2009;125(4):2420–2431. [PubMed: 19354416]

Khokhlova V, Bailey M, Reed J, Cunitz B, Kaczkowski P, Crum L. Effects of nonlinear propagation, cavitation, and boiling in lesion formation by high intensity focused ultrasound in a gel phantom. J Acoust Soc Am 2006;119(3):1834–1848. [PubMed: 16583923]

Khokhlova, V.; Canney, M.; Bailey, M.; Crum, L. Efficient heating and localized millisecond boiling in tissue phantoms by high intensity focused ultrasound due to formation of shocks. 19th International Congress on Acoustics; Madrid, Spain. September 2–7 2007;

Kreider, W. Ph.D. thesis. University of Washington; 2008. Gas-Vapor Bubble Dynamics in Therapeutic Ultrasound.

Kurganov A, Tadmor E. New High-Resolution Central Schemes for Nonlinear Conservation Laws and Convection-Diffusion Equations. J Comp Phys 2000;160:241–282.

Kuznetsov V. Equations of nonlinear acoustics. Sov Phys Acoust 1971;16(4):467–470.

Lafon C, Zderic V, Noble M, Yuen J, Kaczkowski P, Sapozhnikov O, Chavrier F, Crum L, Vaezy S. Gel phantom for use in high-intensity focused ultrasound dosimetry. Ultrasound Med Biol 2005;31(10): 1383–1389. [PubMed: 16223642]

Leighton, T. The Acoustic Bubble. Academic Press; 1994.

Mast T, Hinkelman L, Orr M, Sparrow V, Waag R. Simulation of ultrasonic pulse propagation through the abdominal wall. J Acoust Soc Am 1997;102(2):1177–1190. [PubMed: 9265762]

Meaney P, Cahill M, ter Haar G. The intensity dependence of lesion position shift during focused ultrasound surgery. Ultrasound Med Biol 2000;26(3):441–450. [PubMed: 10773375]

Morse, P.; Feshbach, H. Methods of theoretical physics, Part I. McGraw-Hill; 1953.

Parsons J, Cain C, Abrams G, Fowlkes J. Pulsed cavitational ultrasound therapy for controlled tissue homogenization. Ultrasound Med Biol 2006;32(1):115–29. [PubMed: 16364803]

Pierce, A. Acoustics: An Introduction to Its Physical Principles and Applications. Acoustical Society of America; 1991.

Pishchalnikov Y, Sapozhnikov O, Sinilo T. Increase in the efficiency of the shear wave generation in gelatin due to the nonlinear absorption of a focused ultrasonic beam. Acoust Phys 2002;48(2):214–219.

Plesset M, Zwick S. The Growth of Vapor Bubbles in Superheated Liquids. J Appl Phys 1954;25(4):493–500.

Rabkin B, Zderic V, Crum L, Vaezy S. Biological and Physical Mechanisms of HIFU-Induced Hyperecho in Ultrasound Images. Ultrasound Med Biol 2006;32(11):1721–1729. [PubMed: 17112958]

Sokka S, King R, Hynynen K. MRI-guided gas bubble enhanced ultrasound heating in in vivo rabbit thigh. Phys Med Biol 2003;48:223–241. [PubMed: 12587906]

Thomas, C.; Farny, C.; Wu, T.; Holt, R.; Roy, R. In: Clement, G.; McDannold, N.; Hynynen, K., editors. Monitoring HIFU Lesion Formation In Vitro Via the Driving Voltage; Therapeutic Ultrasound: 5th International Symposium on Therapeutic Ultrasound; American Institute of Physics; 2006. p. 293-297.

Vaezy S, Andrew M, Kaczkowski P, Crum L. Image-guided acoustic therapy. Annu Rev Biomed Eng 2001;3:375–390. [PubMed: 11447068]

Watkin N, ter Haar G, Rivens I. The intensity dependence of the site of maximal energy deposition in focused ultrasound surgery. Ultrasound Med Biol 1996;22(4):483–491. [PubMed: 8795175]

Wu F, Wang Z, Chen W, Zou J, Bai J, Zhu H, Li K, Xie F, Jin C, Su H, Gao G. Extracorporeal Focused Ultrasound Surgery for Treatment of Human Solid Carcinomas: Early Chinese Clinical Experience. Ultrasound Med Biol 2004;30(2):245–260. [PubMed: 14998677]

Zabolotskaya E, Khokhlov R. Quasi-plane waves in the nonlinear acoustics of confined beams. Sov Phys Acoust 1969;15:35–40.

Zhou Y, Zhai L, Simmons R, Zhong P. Measurement of high intensity focused ultrasound fields by a fiber optic probe hydrophone. J Acoust Soc Am 2006;120(2):676–685. [PubMed: 16938956]

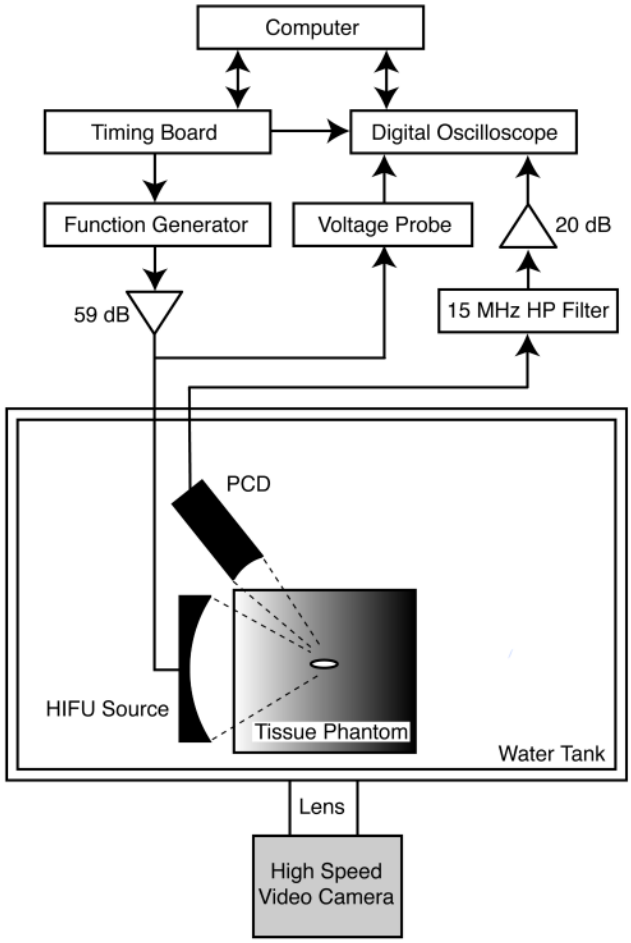

Figure 1.
A diagram of the experimental arrangement used for observing initiation of boiling in tissue-mimicking transparent gel phantoms and *ex vivo* liver samples.

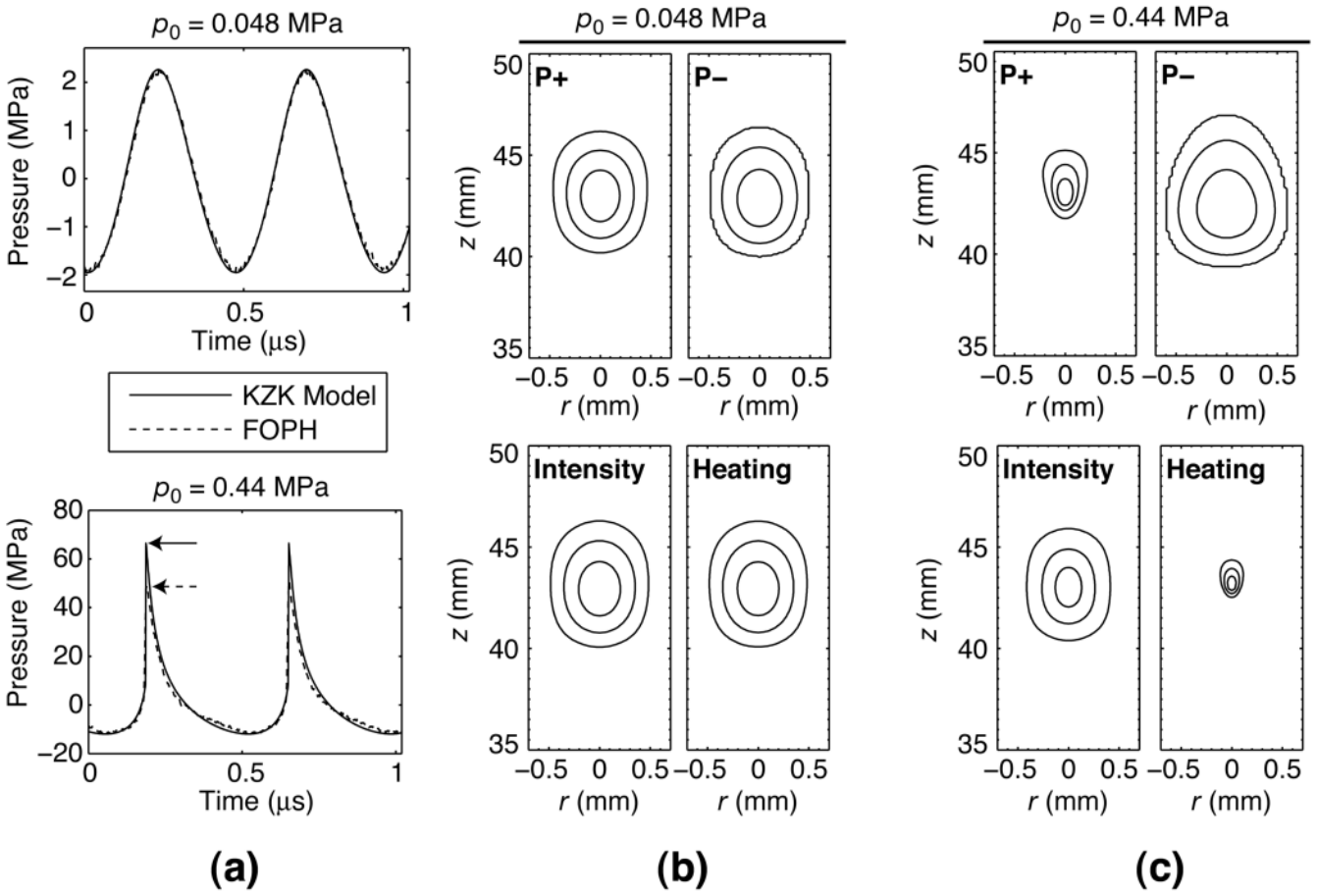

Figure 2.

Measurement and modeling of the acoustic field of the 2-MHz HIFU source in a tissue-mimicking gel phantom containing 7% w/v BSA at two different output levels: p_0=0.048 MPa (I_L=144 W/cm^2, I_N =145 W/cm^2) and p_0=0.44 MPa (I_L=12,000 W/cm^2, I_N =16,700 W/cm^2). (a) Focal waveforms measured using the FOPH and simulated using the KZK model. (b, c) Simulated 2D axial distributions of peak positive and negative pressures, heating, and intensity for an output level where propagation is nearly linear (p_0=0.048 MPa); and for an output level where shocks are formed at the focus (p_0=0.44 MPa). The contours in the 2D distributions depict the −1, −3, and −6 dB regions of each plotted variable.

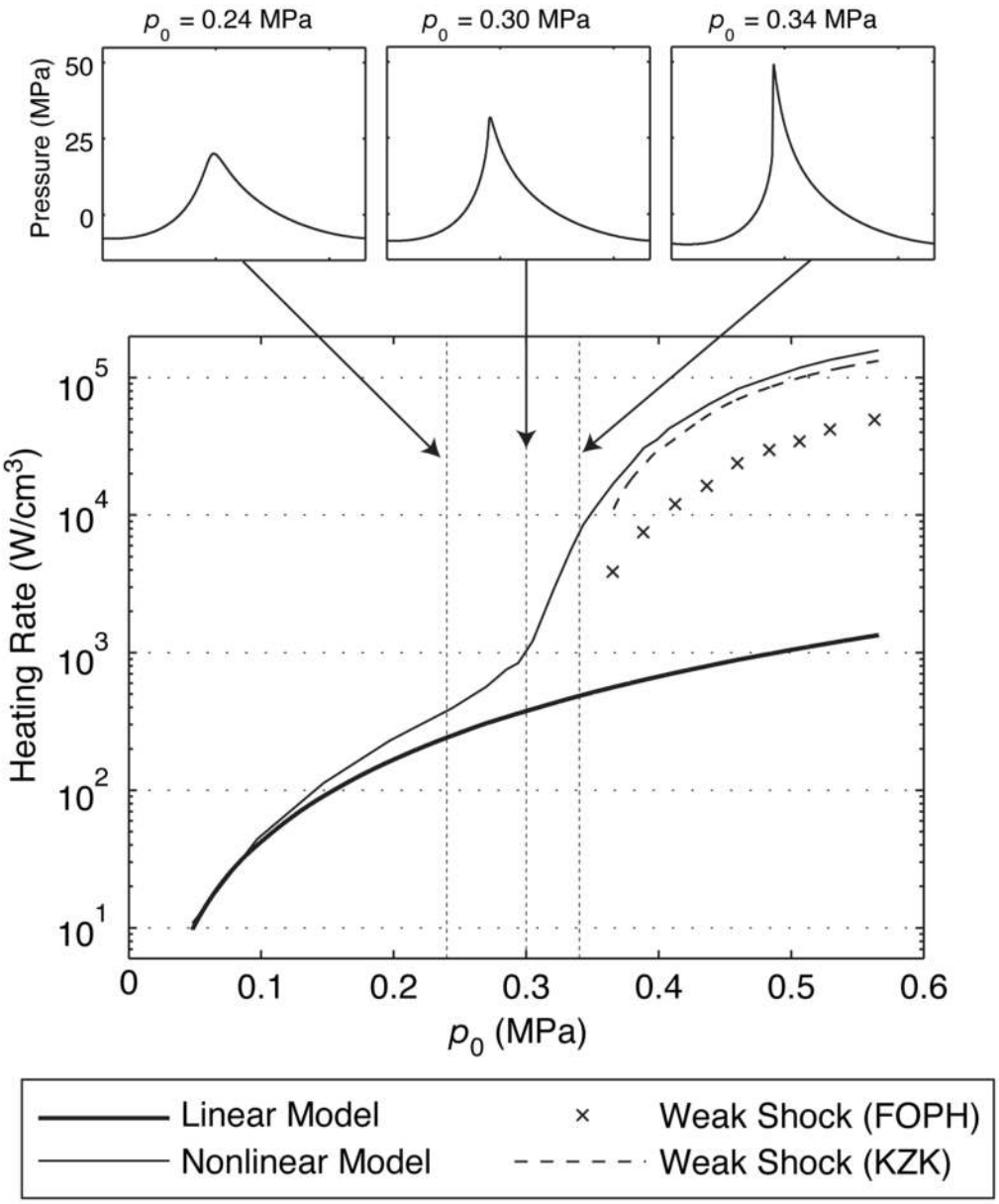

Figure 3.

Peak focal heating rates in gel phantom modeled assuming either linear or nonlinear propagation and calculated using weak shock theory from the modeled and measured focal waveforms. In addition, the peak focal waveforms predicted using the nonlinear model for output levels corresponding to p_0=0.24 MPa, p_0=0.30 MPa, and p_0=0.34 MPa are shown at the top of the figure. A moderate increase in focal heating relative to the linearly predicted heating is observed up until the output where shocks begin to form (p_0=0.30 MPa), at which point the heating rate increases dramatically to a maximum enhancement of 83 times linear predictions.

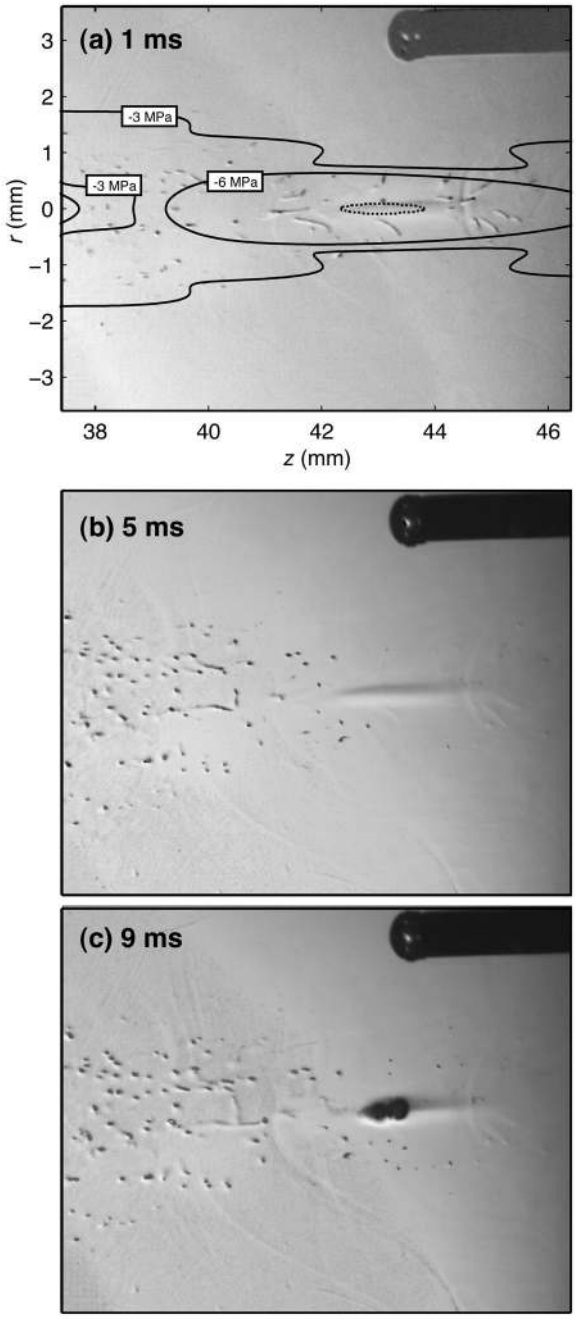

Figure 4.

Observations of cavitation and boiling in a 7% BSA gel phantom. The frames were recorded after (a) 1 ms, (b) 5 ms, and (c) 9 ms of heating at an output level of p_0=0.44 MPa (I_L=12,000 W/cm^2, I_N =16,700 W/cm^2). Boiling occurred after 9 ms of heating and is visible by the formation of a large, millimeter-sized bubble at the focus. In addition, Fig. 4a is combined with an overlay of the simulated 2D axial pressure distributions. The innermost ellipse (dashed curve) indicates the −6 dB region of the peak positive pressure, which also corresponds to the region within the focus where the heating rates are the highest. The contour plots for the peak negative pressure levels of −3 MPa and −6 MPa (solid curves) correspond to the range of cavitation thresholds measured in the gel. Cavitation and boiling bubbles in transparent gel are

visually distinct in size and location. Onset of boiling is observed at the focus of the HIFU source, while cavitation bubbles are observed over a much larger region prefocally.

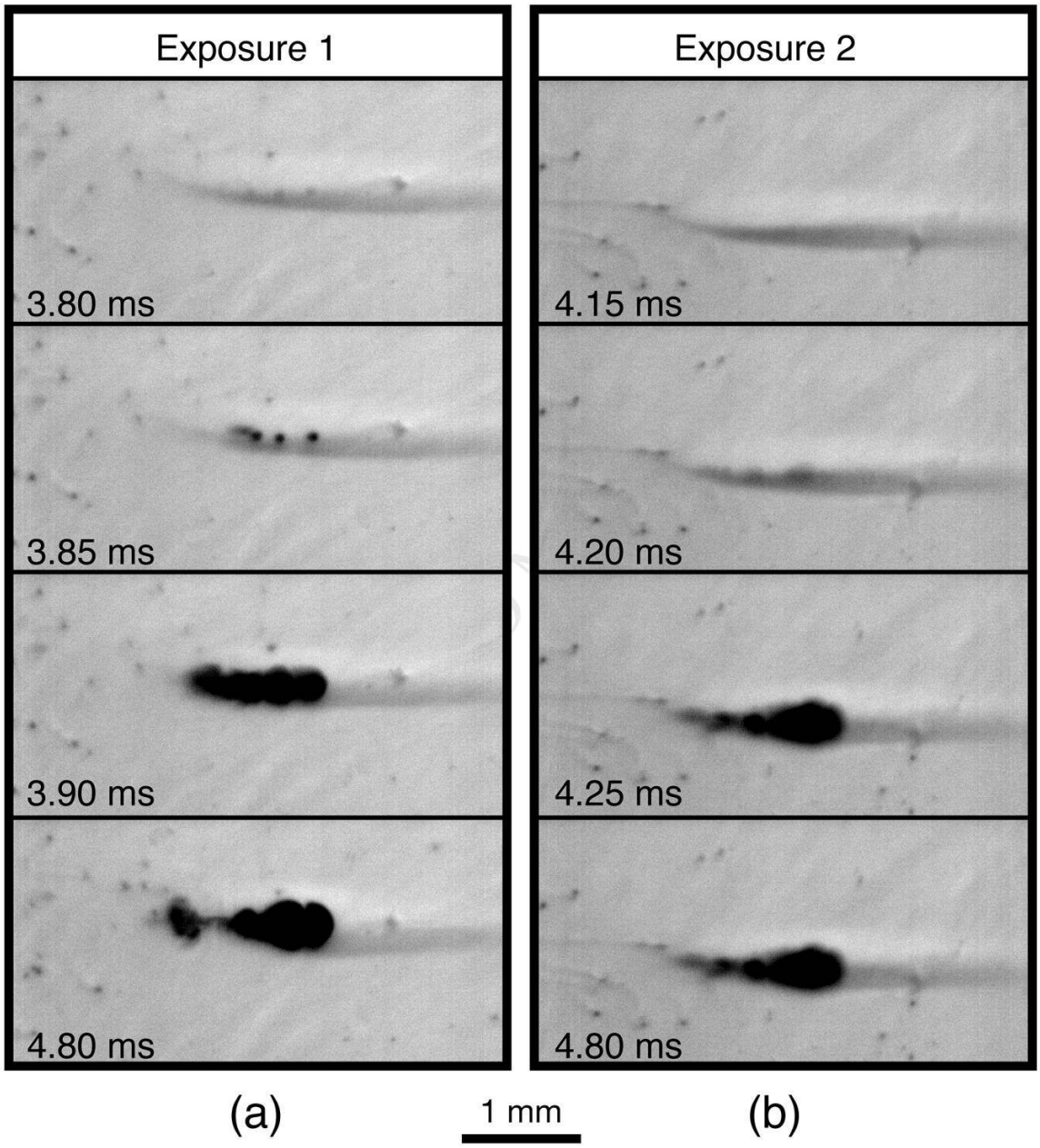

Figure 5.

Selected high-speed movie frames from two separate experiments depicting initiation of boiling in a 7% BSA gel phantom at an output level of p_0=0.57 MPa (I_L=20,000 W/cm^2, I_N =25,500 W/cm^2). In the first experiment (a), visible bubble nuclei appear before boiling and boiling occurs in 3.90 ms. In the second experiment (b), no visible nuclei are seen, implying that boiling started from smaller nuclei than in (a) and boiling occurred after 4.25 ms.

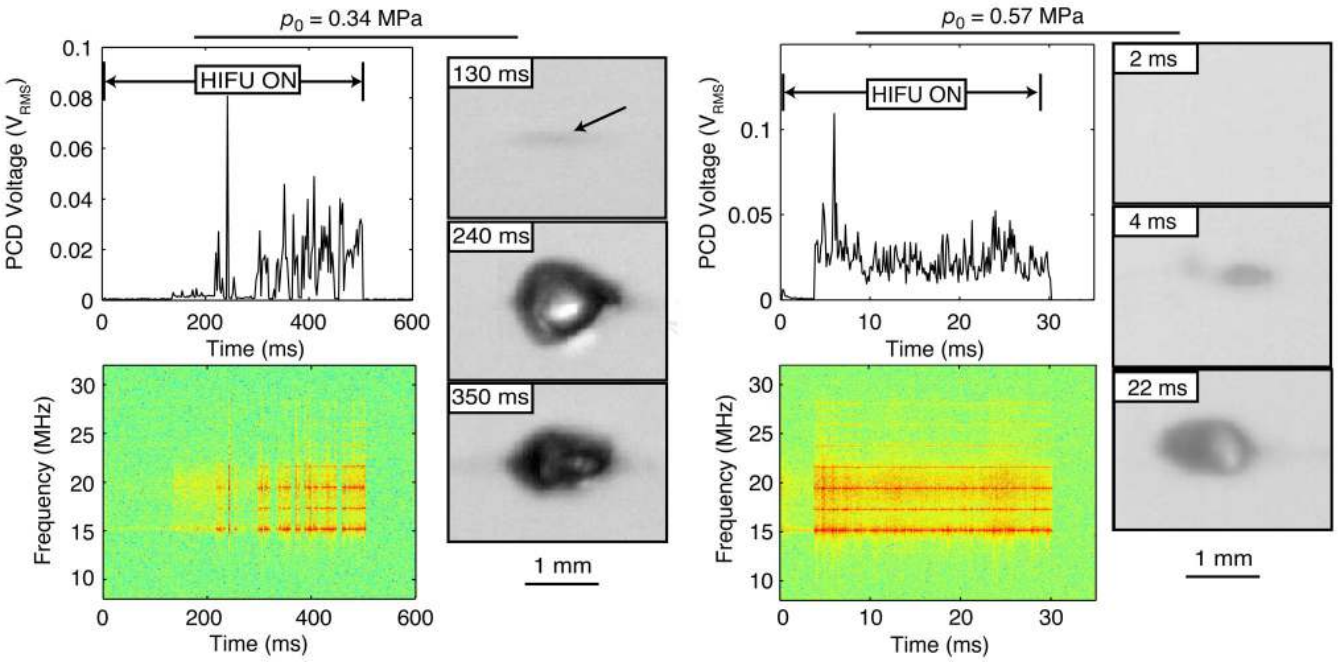

Figure 6.

Experimental observations during 500 ms of HIFU insonation at an output level of p_0=0.34 MPa (I_L=7,300 W/cm^2, I_N =9,600 W/cm^2) and 30 ms at p_0=0.57 MPa (I_L=20,000 W/cm^2, I_N =25,500 W/cm^2) in a gel phantom. The figures on the left of each set show the RMS voltage of the 20-MHz PCD detector [top] and the corresponding spectrogram during the heating [bottom]. The pictures on the right at each power level show the observations from the high-speed video camera at the HIFU focus, filming at 20,000 fps, at selected time points during insonation. At the lower power exposure, boiling occurs at 240 ms of HIFU heating as indicated by the formation of a millimeter-sized bubble at the focus, and also evident by a large increase in signal to the PCD detector. At the higher output level, boiling occurs in 4 ms. Cavitation was detected from the very beginning of insonation, in tens of μs, as broadband noise by the PCD, but was significantly lower in amplitude compared to the signal received when boiling occurred.

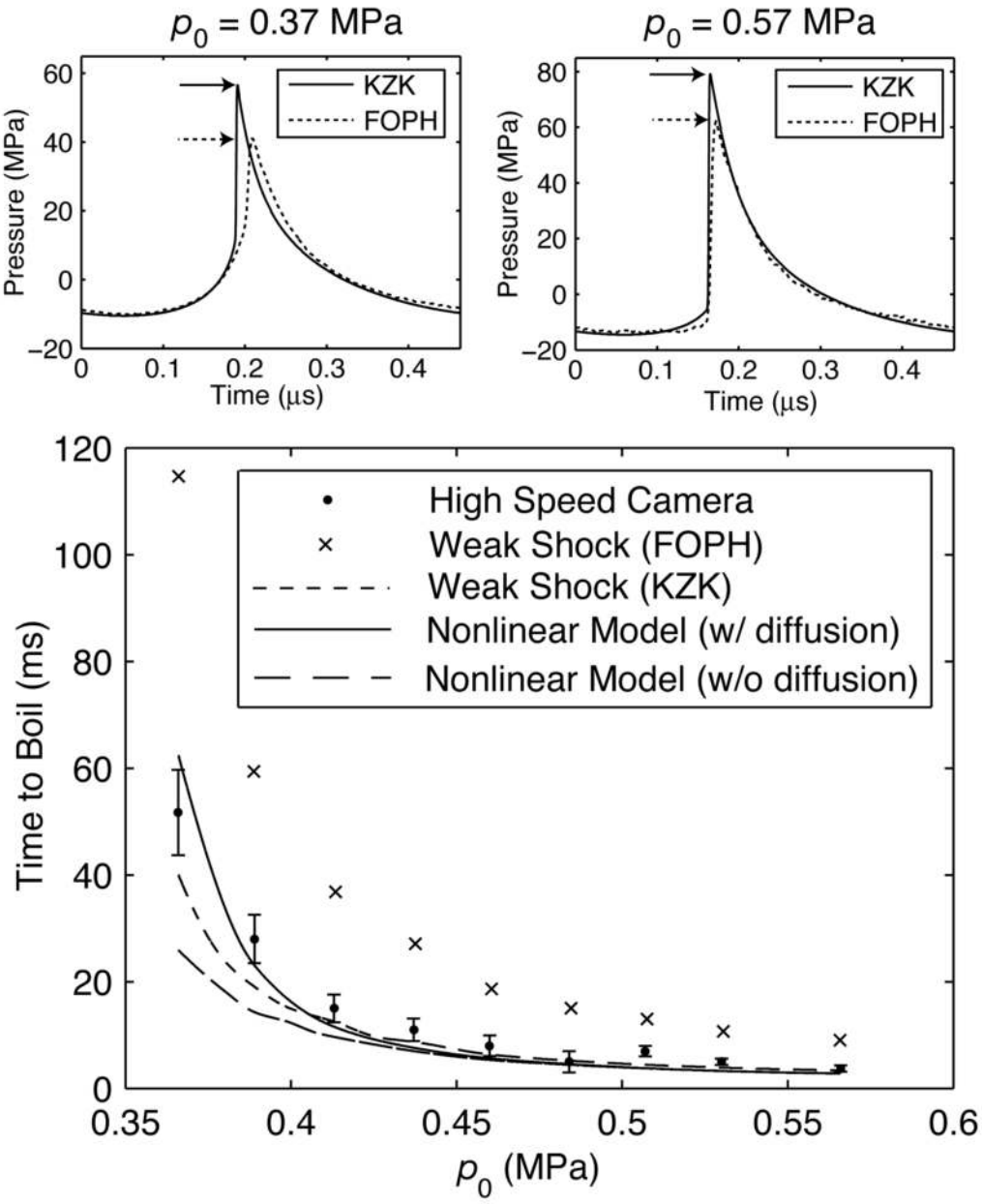

Figure 7.

[top] Focal waveforms measured and modeled for the lowest (p_0=0.39 MPa, I_L= 9,400 W/cm^2, I_N =13,000 W/cm^2) and the highest (p_0=0.57 MPa, I_L=20,000 W/cm^2, I_N =25,500 W/cm^2) output levels where shocks were present at the focus. [bottom] Summary of results from boiling experiments in a 7% BSA gel phantom. The error bars on the high-speed camera data indicate the standard deviation of 5 data points obtained at each source pressure level. The time to boil was calculated from the measured and simulated focal waveforms using weak shock theory, as well as from the full modeling of the nonlinear acoustic field combined with the bioheat equation. No effect of diffusion was observed in modeling results when boiling started in less than 20 ms. At the highest power level, the onset of boiling was detected in less than 4 ms.

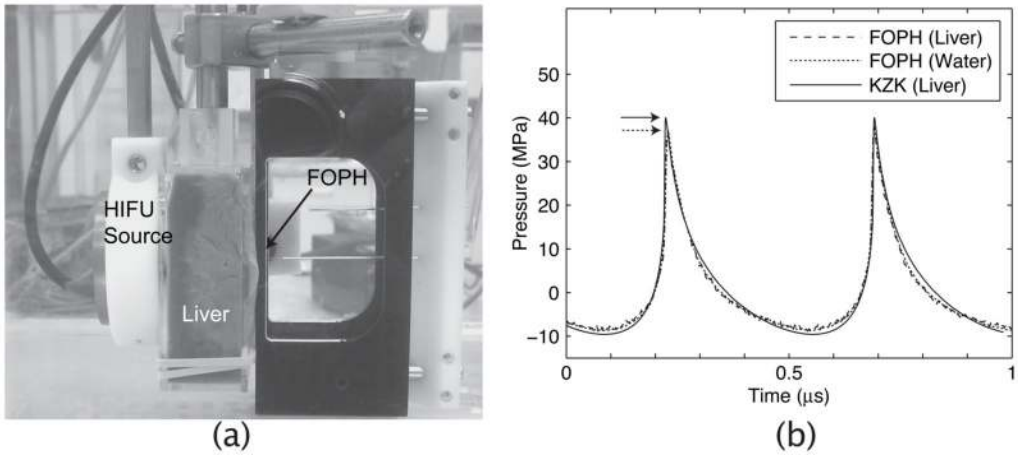

Figure 8.

(a) Photograph of the experimental arrangement for measurement of focal waveforms in *ex vivo* bovine liver. (b) Focal waveform measured after propagation through a 27-mm thick sample at $p_0 = 0.49$ MPa ("FOPH (Liver)") compared with the focal waveform measured in water at $p_0 = 0.29$ MPa ("FOPH (Water)"). By matching experimental focal waveforms obtained in water and behind the liver sample, the attenuation of liver was determined as 1.6 dB/cm at 2.158 MHz. Simulation of the focal waveform in liver ("KZK (Liver)") using the nonlinear model and experimentally determined attenuation agrees well with the experimental data.

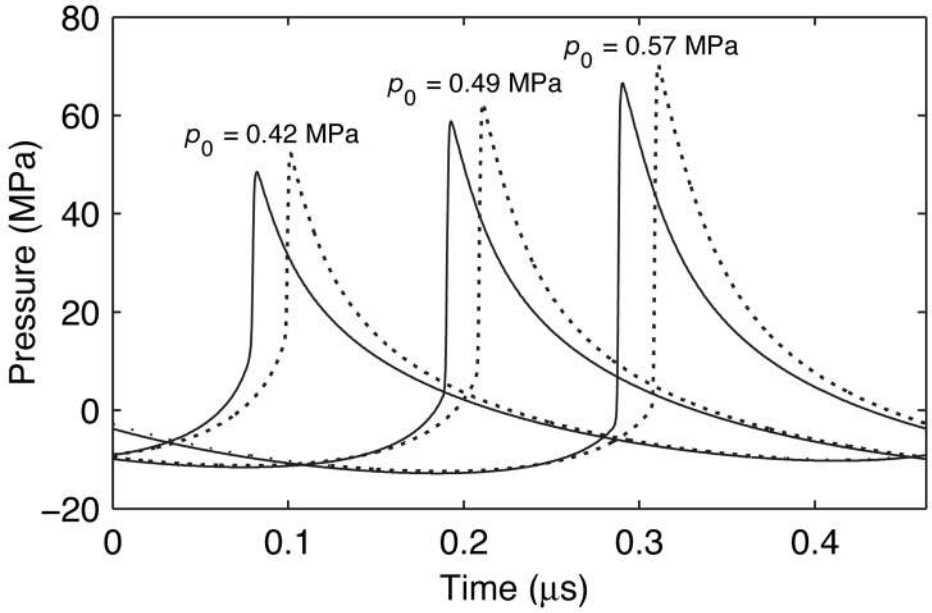

Figure 9.

Focal waveforms modeled in liver (solid curves) and derated from simulations in water (dashed curves) for output levels of p_0=0.42 MPa, 0.49 MPa, and 0.57 MPa at a depth of 13.5 mm in liver tissue. The peak positive pressures in the derated waveforms were slightly higher than those for the simulations in liver; however, the shock amplitudes A_s in the corresponding waveforms were equal.

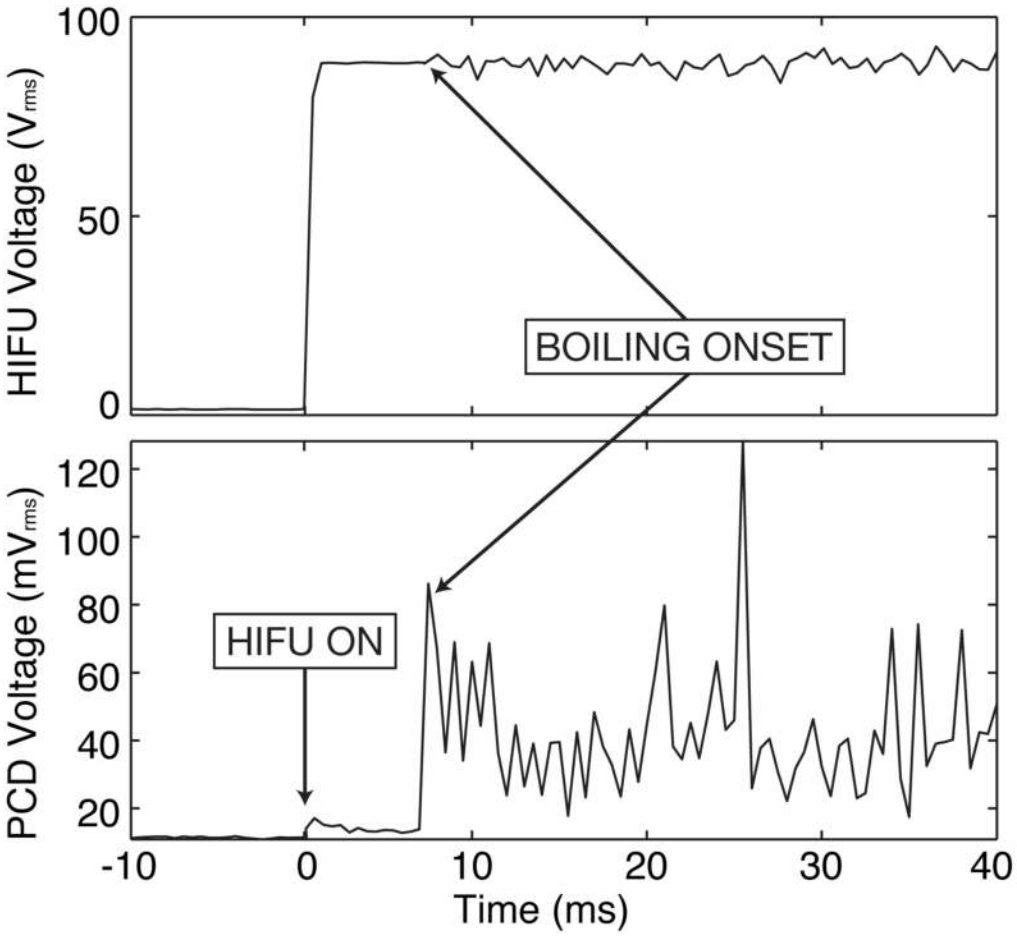

Figure 10.

Detection of boiling in 7.5 ms in liver tissue with the HIFU source operating at p_0=0.49 MPa (I_L=11,400 W/cm^2, I_N =15,200 W/cm^2). The HIFU focus was at a depth of 13.5 mm in the sample. The onset of boiling was observed as fluctuations in the HIFU drive voltage [top] as well as by a large change in the PCD signal amplitude [bottom].

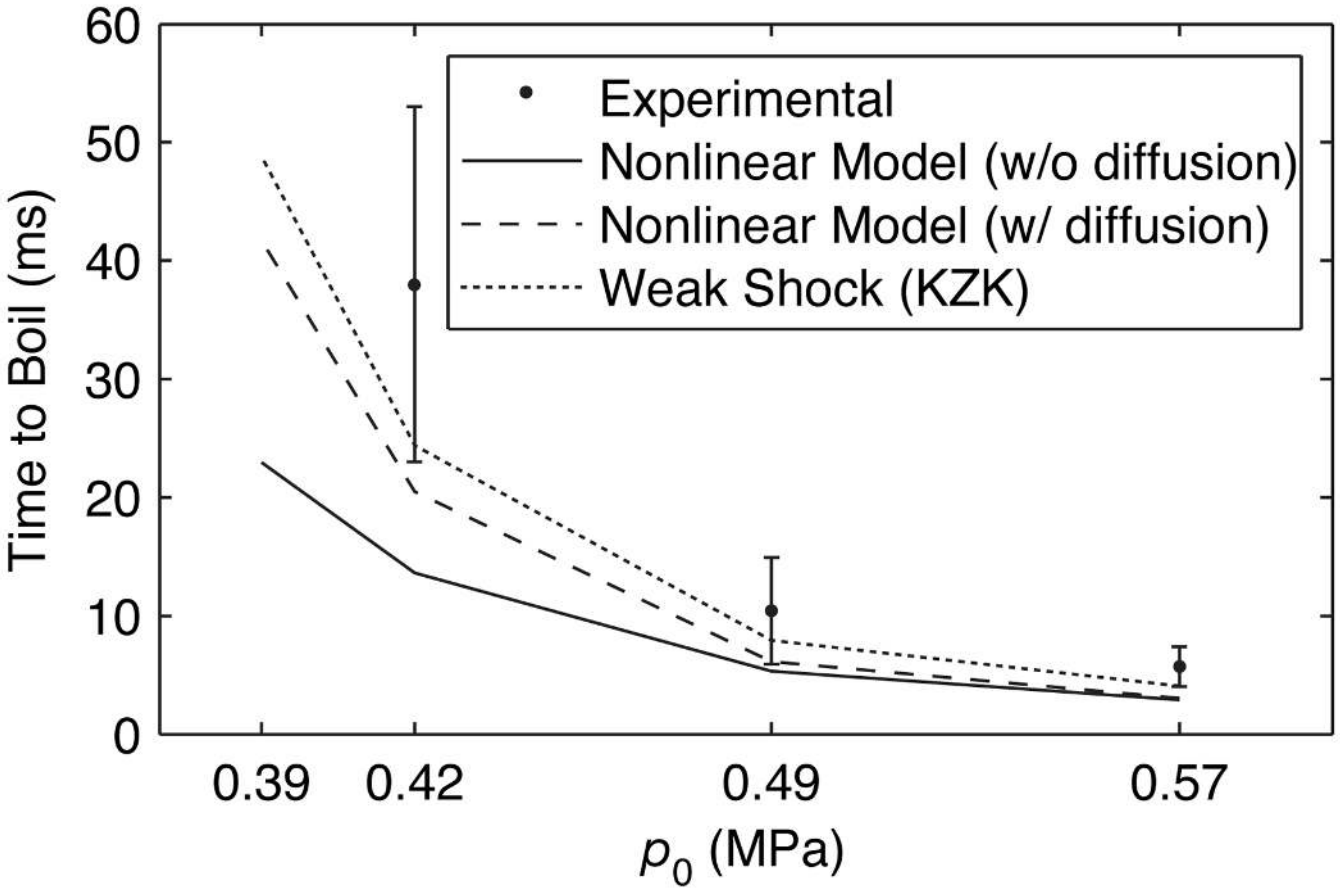

Figure 11.

(a) Summary of time to boil in *ex vivo* bovine liver at three different output levels: p_0=0.42 MPa (I_L=8,400 W/cm^2, I_N =11,100 W/cm^2), p_0=0.49 MPa (I_L=11,300 W/cm^2, I_N =15,200 W/cm^2), and p_0=0.57 MPa (I_L=15,400 W/cm^2, I_N =20,100 W/cm^2). The HIFU focus was at a depth of 13.5 mm in the liver sample. At the highest output level, boiling was observed in as little as 5 ms. Calculations of time to boil agreed well with measurements.

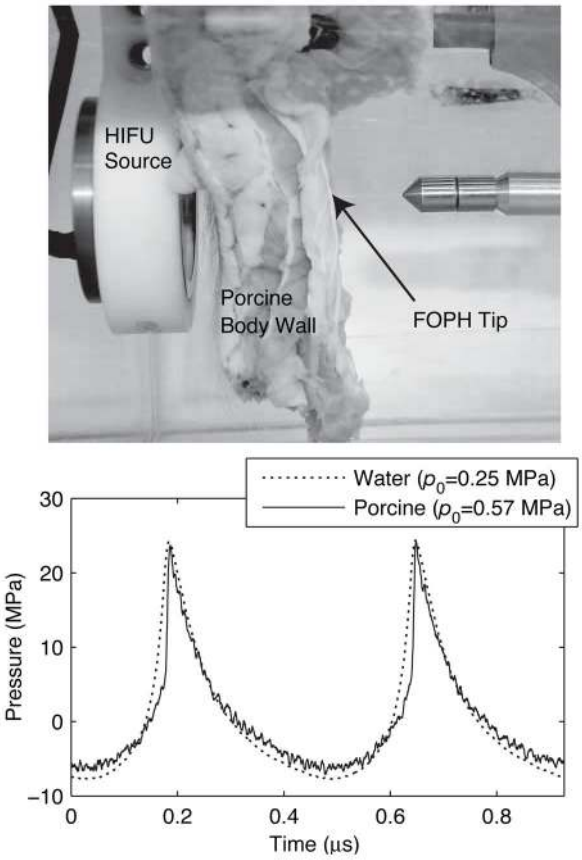

Figure 12.

Measurements of the focal waveform through porcine body wall using the FOPH. The HIFU source was operated at $p_0 = 0.57$ MPa. The focal waveform measured after propagation through inhomogeneous tissue agrees well with measurements in water at $p_0 = 0.25$ MPa, which corresponds to a lumped attenuation of 7.2 dB for the tissue path.